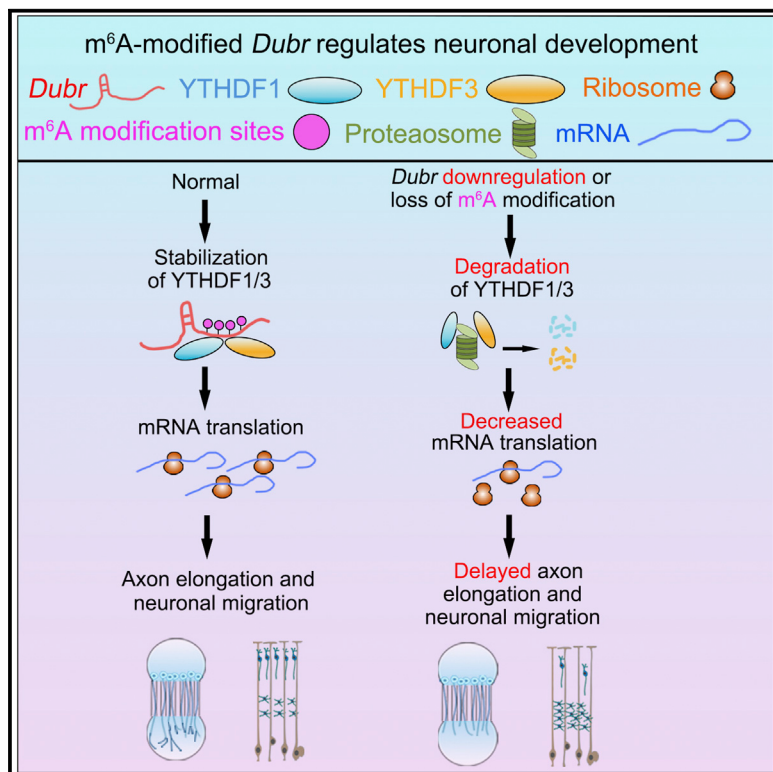


m⁶A-modified lincRNA Dubr is required for neuronal development by stabilizing YTHDF1/3 and facilitating mRNA translation

Graphical abstract



Authors

Jiansong Huang, Bowen Jiang,
Guo-Wei Li, ..., Li Yang, Lan Bao,
Bin Wang

Correspondence

baolan@sibcb.ac.cn (L.B.),
wangbin@gdiist.cn (B.W.)

In brief

Huang et al. find that the m⁶A-modified lincRNA *Dubr* binds and stabilizes the YTHDF1/3 complex through its m⁶A modification, thereby facilitating the translation of Tau and Calmodulin, as well as maintaining subsequent axon elongation and neuronal migration. The findings provide insight into how m⁶A-modified lincRNA orchestrates neuronal development.

Highlights

- m⁶A-modified lincRNA *Dubr* is required for neuronal development
- *Dubr* binds and stabilizes YTHDF1/3 via its m⁶A modification sites
- m⁶A-modified *Dubr* stabilizes the YTHDF1/3 complex and facilitates mRNA translation



Article

m⁶A-modified lincRNA *Dubr* is required for neuronal development by stabilizing YTHDF1/3 and facilitating mRNA translation

Jiansong Huang,¹ Bowen Jiang,¹ Guo-Wei Li,³ Dandan Zheng,⁴ Mingyi Li,¹ Xuan Xie,¹ Yuxiang Pan,¹ Manyi Wei,¹ Xiaoyan Liu,⁶ Xingyu Jiang,⁶ Xu Zhang,^{2,5,7} Li Yang,⁸ Lan Bao,^{1,4,*} and Bin Wang^{1,2,9,*}

¹State Key Laboratory of Cell Biology, Shanghai Institute of Biochemistry and Cell Biology, CAS Center for Excellence in Molecular Cell Science, Chinese Academy of Sciences, University of Chinese Academy of Sciences, Shanghai 200031, China

²Guangdong Institute of Intelligence Science and Technology, Hengqin 519031, Zhuhai, China

³CAS Key Laboratory of Computational Biology, Shanghai Institute of Nutrition and Health, Chinese Academy of Sciences, Shanghai 200031, China

⁴School of Life Science and Technology, ShanghaiTech University, Shanghai 201210, China

⁵Institute of Neuroscience and State Key Laboratory of Neuroscience, CAS Center for Excellence in Brain Science and Intelligence Technology, Shanghai 200031, China

⁶Southern University of Science and Technology, Shenzhen 518055, China

⁷Shanghai Advanced Research Institute, Chinese Academy of Sciences, Shanghai 201210, China

⁸Center for Molecular Medicine, Children's Hospital, Fudan University and Shanghai Key Laboratory of Medical Epigenetics, International Laboratory of Medical Epigenetics and Metabolism, Ministry of Science and Technology, Institutes of Biomedical Sciences, Fudan University, Shanghai 200031, China

⁹Lead contact

*Correspondence: baolan@sibcb.ac.cn (L.B.), wangbin@gdiist.cn (B.W.)

<https://doi.org/10.1016/j.celrep.2022.111693>

SUMMARY

Long intergenic noncoding RNAs (lncRNAs) are crucial regulators in numerous biological processes. However, the functions and mechanisms of m⁶A-modified lncRNAs in neuronal development remain unclear. Here, we report an m⁶A-modified lncRNA, *Dppa2* upstream binding RNA (*Dubr*), abundantly expressed at the early developmental stage of dorsal root ganglion (DRG) and cerebral cortex. Silencing *Dubr* impairs axon elongation of DRG neurons and axon projection and migration of cortical neurons, whereas lacking m⁶A modification of *Dubr* fully loses its functions. Mechanically, *Dubr* interacts with m⁶A-binding proteins, the YTHDF1/3 complex, through its m⁶A motifs to protect YTHDF1/3 from degradation via the proteasome pathway. Furthermore, Tau and Calmodulin are regulated by YTHDF1/3 and m⁶A-modified *Dubr*. Overexpression of YTHDF1/3 not only rescues the reduced Tau and Calmodulin but also restores axon elongation of DRG neurons by *Dubr* knockdown. This study uncovers a critical role of m⁶A-modified lncRNA in neuronal development by regulating the degradation of RNA-binding protein.

INTRODUCTION

Development of the mammalian nervous system is a complicated process, including neurogenesis, neuronal differentiation, and migration, as well as axon growth and synaptogenesis, which enables the establishment of neuronal connectivity and functions (Komuro and Rakic, 1998; Kosodo and Huttner, 2009; Kriegstein and Noctor, 2004; Taverna et al., 2014). Among these processes, stage-specific regulation of gene expression and protein synthesis are precisely and spatiotemporally required for distinct types of neurons. Recently, high-throughput technologies, such as deep RNA sequencing (RNA-seq) reveal that noncoding RNAs are particularly abundant in the nervous system, and numerous studies suggest noncoding RNAs as versatile regulators in the gene expression and related functions (Costa, 2010; Qureshi et al., 2010; Wang et al., 2008; Zhao et al., 2013).

Accumulated evidence reveals that long noncoding RNAs (lncRNAs), defined as transcripts longer than 200 nucleotides (nt) without encoding proteins, serve as key regulators in the development, plasticity, and disease of the mammalian nervous system (Aprea et al., 2013; Briggs et al., 2015; Mus et al., 2007; Muslimov et al., 1998; Ng et al., 2013; Quan et al., 2017; Wu et al., 2013; Zhao et al., 2013). Bioinformatic analysis of multi-omic data also show that long intergenic noncoding RNAs (lncRNAs), which are transcribed from the intergenic region and constitute half of lncRNAs, are particularly tissue- and cell-type-specific, especially for the nervous system (Khalil et al., 2009; Yoon et al., 2017). Recent studies further report the crucial roles of lncRNAs, such as *Pnky* and *TUNA*, in neuronal differentiation (Guo et al., 2018; Ramos et al., 2015), ALAE in axon elongation (Wei et al., 2021), and *Slic1* in nerve regeneration (Perry et al., 2018). The majority of studies suggest that lncRNAs exert their



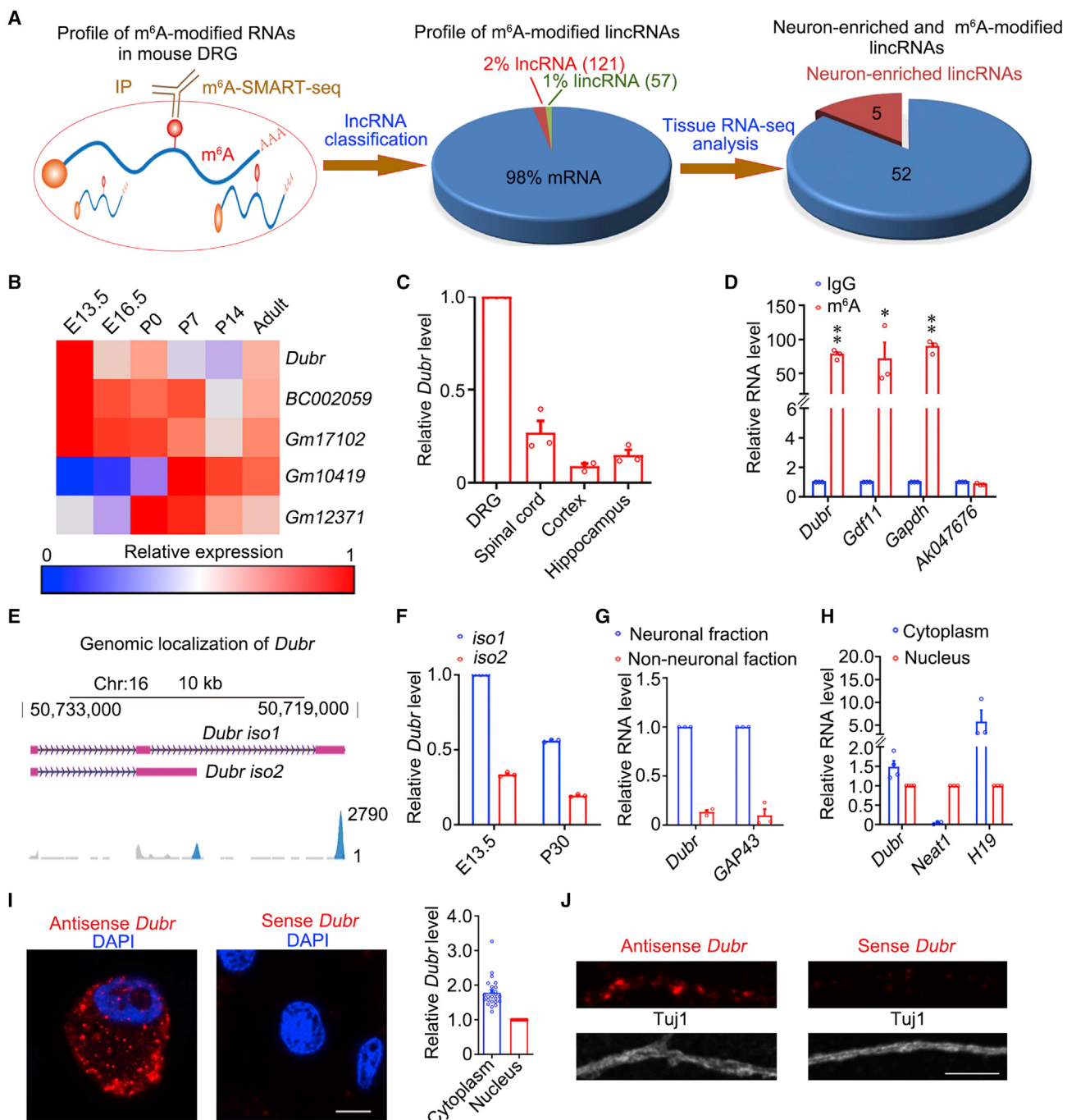


Figure 1. m⁶A-modified and cytoplasm-enriched lncRNA *Dubr* is highly expressed at early-stage development of DRG neurons

(A) Research flowchart for characterizing m⁶A-modified lncRNAs from m⁶A-SMART-seq. The pie chart showed that 5 of 57 methylated lncRNAs were identified as neuron-enriched lncRNAs by RNA-seq data of mouse tissues from the Ensemble database.

(B) Heatmap by qPCR showed that *Dubr* was highly expressed at the early stage of mouse DRG development among five neuron-enriched lncRNAs. *Gm10419* was greatly expressed at postnatal stage of P7 and P14, whereas *BC002059* and *Gm17102* evenly expressed at embryonic stages of DRG. The relative expression level for individual lncRNA at different stages were calculated by normalizing to its highest expression stage.

(C) qPCR analysis showed that *Dubr* was relatively more abundant in the DRG than other tissues, including spinal cord, cortex, and hippocampus at P0 mice. n = 3.

(D) qPCR showed that *Dubr* was highly enriched in the m⁶A immunoprecipitates of P0 DRGs. *Gdf11* and *Gapdh* served as positive controls. *Ak047676* served as a negative control. IgG served as control. n = 3. *p < 0.05, **p < 0.01 versus IgG.

(E) 10x Genomics scRNA-seq of DRG neurons showing the genomic localization for two splicing forms of *Dubr*.

(legend continued on next page)

roles by regulating transcription in the nucleus and posttranscriptional functions, such as mRNA stability and translation in the cytoplasm (Yao et al., 2019). However, this is still unexplored for lncRNA-mediated functions via the RNA modification in distinct biological processes.

N6-Methyladenosine (m^6A) is the most abundant internal modification found within eukaryotic mRNAs (Desrosiers et al., 1974). The dynamic and reversible m^6A modification is regulated by methyltransferases (“writers”), demethylating enzymes (“erasers”), and the proteins that recognize the m^6A transcripts (“readers”) (Widagdo and Anggono, 2018). m^6A modification has been implicated in many biological processes, including RNA processing, translation (Wang et al., 2015c), and decay (Fu et al., 2014). Recent studies report that m^6A modification is highly enriched in the nervous system and plays crucial roles in neurogenesis, neuronal differentiation (Yoon et al., 2017), and axon guidance (Yu et al., 2018), as well as learning and memory (Shi et al., 2018). Furthermore, analysis of m^6A -modified RNAs by RNA-seq after peripheral nerve injury shows a dynamic m^6A landscape, and loss of methyltransferases Mettl14 and m^6A reader protein YTHDF1 attenuates injury-induced protein translation and reduces axon regeneration (Weng et al., 2018). Nevertheless, the roles and related mechanisms of m^6A -methylated lncRNAs remain unclear during the development of the nervous system.

In the present study, based on the profile of m^6A -modified lncRNAs in the mouse dorsal root ganglion (DRG) (Weng et al., 2018), we identified a highly m^6A -modified and neuron-expressed lncRNA, *Dppa2* upstream binding RNA (*Dubr*). This lncRNA regulated axon elongation of DRG neurons as well as axon projection and migration of cortical neurons. Importantly, *Dubr* interacts with YTHDF1/3 through its m^6A motifs to protect their degradation, thereby facilitating the YTHDF1/3-mediated translation of Tau and Calmodulin, and subsequent neuronal migration and axon elongation. Our study highlights a regulatory role of methylated lncRNA in neuronal development.

RESULTS

***Dubr* is an m^6A -modified and cytoplasm-enriched lncRNA highly expressed at early-stage development of DRG neurons**

Several studies have uncovered crucial roles of m^6A modification in the RNA during neuronal development (Shi et al., 2018; Yu et al., 2018). To obtain the profile of m^6A -modified lncRNAs, we reanalyzed the database of genome-wide profiling for m^6A -tagged transcripts in the DRG of adult mice (Weng et al., 2018) (Figure 1A). In total, 5,963 m^6A -modified RNAs were identified from the SMART-seq data by m^6A -CLIP from mouse DRGs. Among these m^6A -modified RNAs, 121 were characterized as lncRNAs including 57 lncRNAs that are transcribed from intergenic regions and lack protein-coding potential (Figure 1A;

Table S1). Based on the RNA-seq data of mouse tissues from the Ensembl database, 5 of 57 lncRNAs including BC002059, Gm17102, Gm10419, 5330426P16Rik, and Gm12731 display high expression (FPKM > 1) in the nervous system (Figures 1A and S1A). To further screen out the development-related lncRNA, we perform quantitative PCR (qPCR) to examine the expression of these five lncRNAs during DRG development. qPCR showed that the level of 5330426P16Rik, also called *Dubr*, was relatively high at the early stage of mouse DRG (Figures 1B and S1B), implying a potential function of *Dubr* during DRG development. Our previous study showed that cultured postnatal day 0 (P0) of DRG neurons also exhibited rapid axon growth as similar to the embryonic day 13.5 (E13.5) period and more resistant to electroporation than embryonic DRG neurons (Wei et al., 2021). Therefore, we chose the P0 stage to investigate the distribution and m^6A modification of *Dubr*. qPCR also detected that *Dubr* was relatively higher in DRGs than other tissues of the nervous system, including spinal cord, cortex, and hippocampus at P0 mice (Figure 1C). Furthermore, we performed RNA immunoprecipitation (RIP) by m^6A antibody to confirm the methylation of *Dubr* in DRGs. qPCR showed that the high level of *Dubr*, together with the known m^6A -modified mRNAs, including *Gdf11* and *Gapdh* (Weng et al., 2018), was present in the immunoprecipitation of m^6A antibody, not for lncRNA *Ak047676* without m^6A modification (Figure 1D). Meanwhile, we reanalyzed the m^6A -RIP data from mouse brain tissues, as reported previously (Nie et al., 2021), to investigate m^6A -modified lncRNAs in different developmental stages of the cerebral cortex. The m^6A RIP-seq results showed that methylation of *Dubr* was relatively enriched in different regions of 7-week mouse brain including the cerebellum, hypothalamus, and cerebrum, as well as the cortex of E13.5 and P14 mice (Figure S1C), indicating a constitutive m^6A modification of *Dubr* during brain development. Therefore, *Dubr* is constitutively m^6A modified and highly expressed at early-stage development of DRGs.

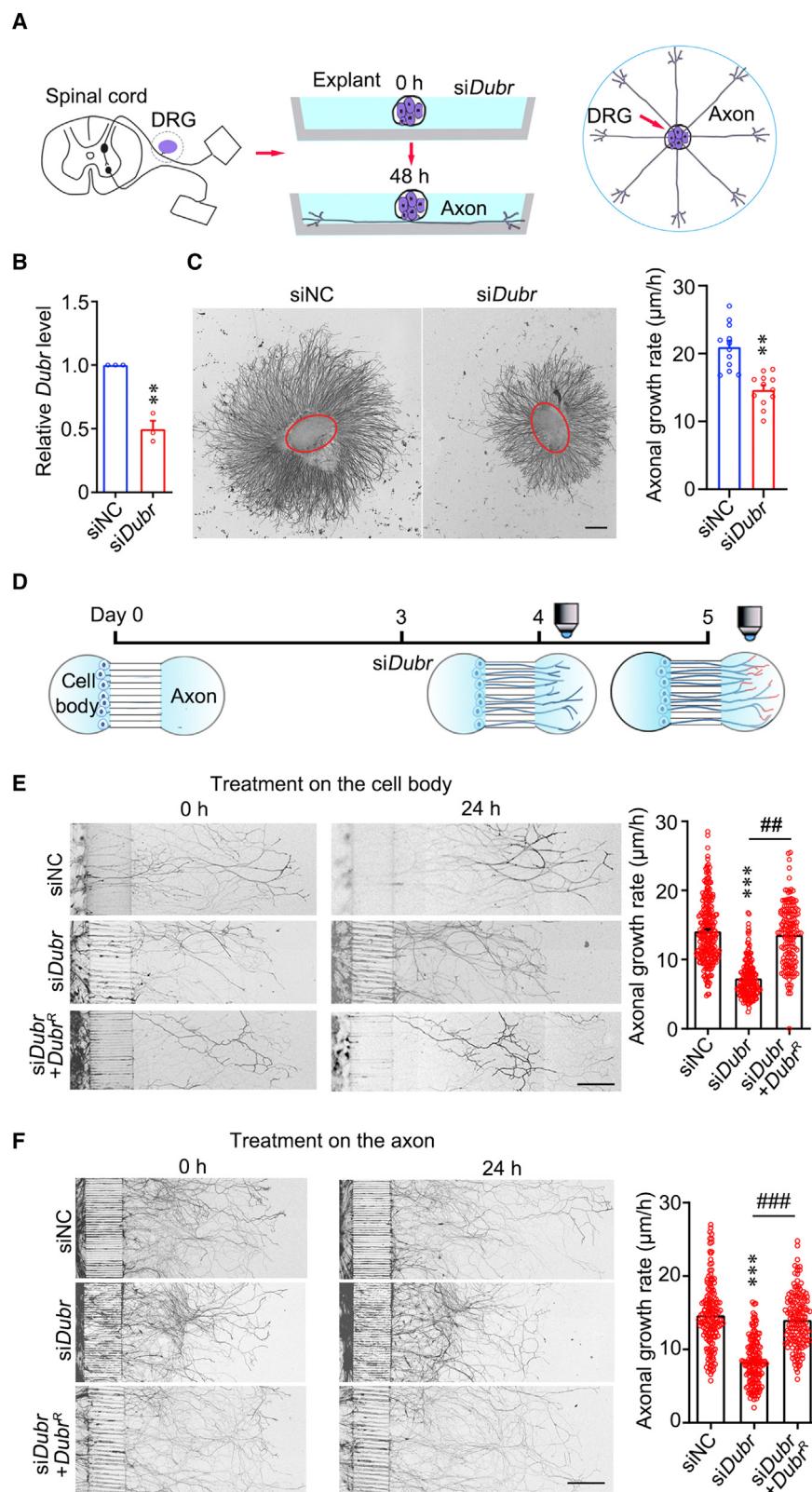
Reanalysis of our single-cell RNA-seq data from DRG neurons by 10x Genomics (Wang et al., 2021a) showed that *Dubr* contained two splicing forms including isoform 1 (iso 1) and isoform 2 (iso 2), which were localized in chromosome 16 (Figure 1E). RNA-seq and PCR showed that the iso1 and iso2 of *Dubr* contained 1,802 nt with 3 exons and 2,919 nt with 2 exons, respectively (Figures 1E and S1D). Two *Dubr* isoforms shared a highly conserved region of ~700 nt between the first and second exon (Figure 1E). qPCR detected that the expression level of *Dubr* iso1 was 3-fold higher than that of *Dubr* iso2 in the DRG at E13.5 and P30 (Figure 1F), similar to the result from 10x Genomics analysis in the DRG at P60 (Figure 1E). Furthermore, to evaluate the coding potential of *Dubr*, we made constructs expressing three predicated open reading frames (ORFs) by inserting an HA tag before the stop codon of each ORF, respectively. Although qPCR showed that the expression levels of these

(F) qPCR showed that the expression level of *Dubr* iso1 was three times higher than iso2 at E13.5 and P30 DRGs. n = 3.

(G) qPCR showed that *Dubr* was specifically distributed in the neuronal fraction marked by *Gap43* mRNA, a neuronal marker. n = 3.

(H) qPCR showed that *Dubr* was more enriched in the cytoplasmic fraction, similar as a cytoplasm-enriched lncRNA *H19*. n = 3.

(I and J) Representative FISH images and quantitative data showed that *Dubr* (red) was more enriched in the cytoplasm (I) (n = 24) and axon (J) of DRG neurons. DAPI (blue) and Tuj1 served as a nuclear and neuronal marker, respectively. Scale bar, 10 μ m. All results are presented as mean \pm SEM. See also Figure S1 and Table S1.



(legend on next page)

constructs were comparable in Neuro 2A (N2A) cells, a mouse neuroblastoma cell line, immunoblotting of HA did not display any protein bands (Figure S1E), suggesting lack of coding potential for these three predicted ORFs. In addition, we performed RIP by antibody of ribosome protein L4 (RPL4), a ribosome sub-unit required for translation elongation (Kakehi et al., 2015). qPCR showed that the level of *Dubr* together with known lncRNA *H19* was not enriched in RPL4 immunoprecipitates, whereas *Gapdh* mRNA was highly enriched (Figure S1F), implying that *Dubr* does not have an ability to encode a protein. Thus, *Dubr* is indeed a lincRNA containing two isoforms.

To determine the cellular expression of *Dubr*, we separated mouse DRG neurons from non-neuronal cells at P0 by Percoll gradients as previously reported (Wei et al., 2021). qPCR showed that *Dubr* was highly enriched in the neuronal fraction marked by the mRNA level of neuronal marker, growth-associated protein 43 (GAP43) (Figure 1G). Further subcellular localization of *Dubr* was examined by biochemical and morphological assays. Biochemical fraction of dissociated DRG neurons at P0 showed that *Dubr* was relatively more enriched in the cytoplasm than in the nucleus (Figure 1H). Meanwhile, immunofluorescence images of *Dubr* by *in situ* hybridization (FISH) exhibited a puncta structure in both cell body and axon of cultured P0 DRG neurons (Figures 1I and 1J). These data suggest that *Dubr* is a cytoplasm-enriched lincRNA in DRG neurons.

Downregulation of *Dubr* decreases axon elongation of DRG neurons

Since the higher expression of *Dubr* in the E13.5 and P0 stages of DRG neurons (Figure 1B), which were implicated as the important periods for rapid axon growth, we accessed the effect of *Dubr* on axon elongation after transfecting small interfering RNA (siRNA) in ex-vivo-cultured P0 DRG explants as reported previously (Li et al., 2012) (Figure 2A). Application of si*Dubr* for 48 h dramatically reduced the expression level of *Dubr* in cultured P0 DRG explants (Figure 2B). Afterward, the axons extending from the DRG explant were measured. Importantly, knockdown of *Dubr* significantly reduced the axon growth rate from ex-vivo-cultured DRG explants (Figure 2C). To precisely examine axon elongation by knockdown of *Dubr*, we performed siRNA experiments in the cell body compartment of microfluidic-cultured P0 DRG neurons as reported previously (Wei et al., 2021) (Figure 2D). Application of si*Dubr* in the cell body compartment reduced the level of *Dubr* in both cell bodies and axons of DRG neurons, while coexpression of siRNA-resistant *Dubr* (*Dubr*^R) fully rescued the decreased level of *Dubr* due to si*Dubr*

treatment (Figure S2A). After siRNA treatment for 24 h, the elongated axons were traced and measured for another 24 h. Notably, knockdown of *Dubr* decreased the axon growth rate, while coexpression of *Dubr* completely rescued the defect caused by si*Dubr* (Figure 2E). Given the higher cytoplasmic and axonal distribution of *Dubr* (Figures 1I and 1J), we sought to determine the local axonal effect of *Dubr* during axon elongation. Application of si*Dubr* in the axon compartment also reduced *Dubr* in axons but not in cell bodies, and coexpression of *Dubr*^R in axons fully rescued the decreased level of axonal *Dubr* (Figure S2B). Meanwhile, knockdown of *Dubr* in axons also decreased the axon growth rate, which was completely rescued by axonal application of *Dubr*^R (Figure 2F), suggesting a local regulation of *Dubr*. In addition, we transfected *Dubr* in the cell body compartment of microfluidic-cultured P0 DRG neurons to examine the effect of *Dubr* overexpression. Despite highly increased *Dubr* detected both in cell bodies and axons (Figure S2C), the axon growth rate was not affected by overexpression of *Dubr* (Figure S2D), implying a ceiling effect of *Dubr* due to its abundance in DRG neurons. Taken together, these data suggest that *Dubr* is required for axon elongation of DRG neurons in the peripheral nerve system.

Downregulation of *Dubr* causes delayed migration and axon projection of cortical neurons

Given the specific and abundant expression of *Dubr* in the central nervous system (Figure S1A), we then sought to investigate the expression level of *Dubr* during cortical development. Analysis of our RNA-seq data from mouse E12 to P30 cortex showed that *Dubr* reached the highest level at E14, whereas other methylated lncRNAs, such as *Gm10419* and *Gm17102*, were abundantly expressed at P30 and P0, respectively (Figure 3A). The developmental stages from E14 to E16 are critical periods for morphological transition and radial migration of cortical neurons (Xie et al., 2021). A previous study reported that *Dubr* is specifically expressed in cortical neurons distributed in the intermediate zone (Elsen et al., 2018) and subventricular zone at E14 (Elsen et al., 2018), implying a potential function of *Dubr* in cortical development. Afterward, we designed a short hairpin RNA (shRNA) targeting to *Dubr* (sh*Dubr*) and detected that the level of *Dubr* was dramatically reduced in cultured cortical neurons transfected with sh*Dubr* (Figure 3B). Utilizing *in utero* electroporation (IUE) in the cerebral cortex of E14 mice, the radial glia progenitors were transfected with the constructs containing shRNA and GFP reporter (Figure 3C). The GFP-positive (GFP⁺) cells were analyzed in the somatosensory cortex at E18, which

Figure 2. *Dubr* downregulation decreases the axon elongation of DRG neurons

- (A) Research flowchart for detection of the axon elongation in cultured mouse P0 DRG explants.
- (B) qPCR showed that the expression of *Dubr* was significantly decreased after transfection of si*Dubr* in cultured P0 DRG explants. n = 3.
- (C) Representative images (left) and quantitative data (right) showed that knockdown of *Dubr* significantly reduced the axon elongation in cultured P0 DRG explants (siNC, n = 13; si*Dubr*, n = 13). Red cycle indicated the profile of DRG. Scale bar, 300 μm.
- (D) Research flowchart for detection of the axon elongation in the microfluidic chamber.
- (E) Representative images (left) and quantitative data (right) showed that knockdown of *Dubr* in the cell body compartment reduced axon elongation, and co-expression of *Dubr*^R in cell bodies completely rescued decreased axon elongation due to si*Dubr* (siNC, n = 251; si*Dubr*, n = 184; si*Dubr* + *Dubr*^R, n = 164). Scale bar, 300 μm. **p < 0.01, ***p < 0.001 versus siNC, and #p < 0.01, ###p < 0.001 versus indicated. All results are presented as mean ± SEM. See also Figure S2.
- (F) Representative images (left) and quantitative analysis (right) showed that knockdown of *Dubr* in the axon compartment reduced axon elongation, and co-expression of *Dubr*^R in axons rescued the decreased axon elongation caused by si*Dubr* (siNC, n = 156; si*Dubr*, n = 150; si*Dubr* + *Dubr*^R, n = 150). Scale bar, 300 μm. **p < 0.01, ***p < 0.001 versus siNC, and #p < 0.01, ###p < 0.001 versus indicated. All results are presented as mean ± SEM. See also Figure S2.

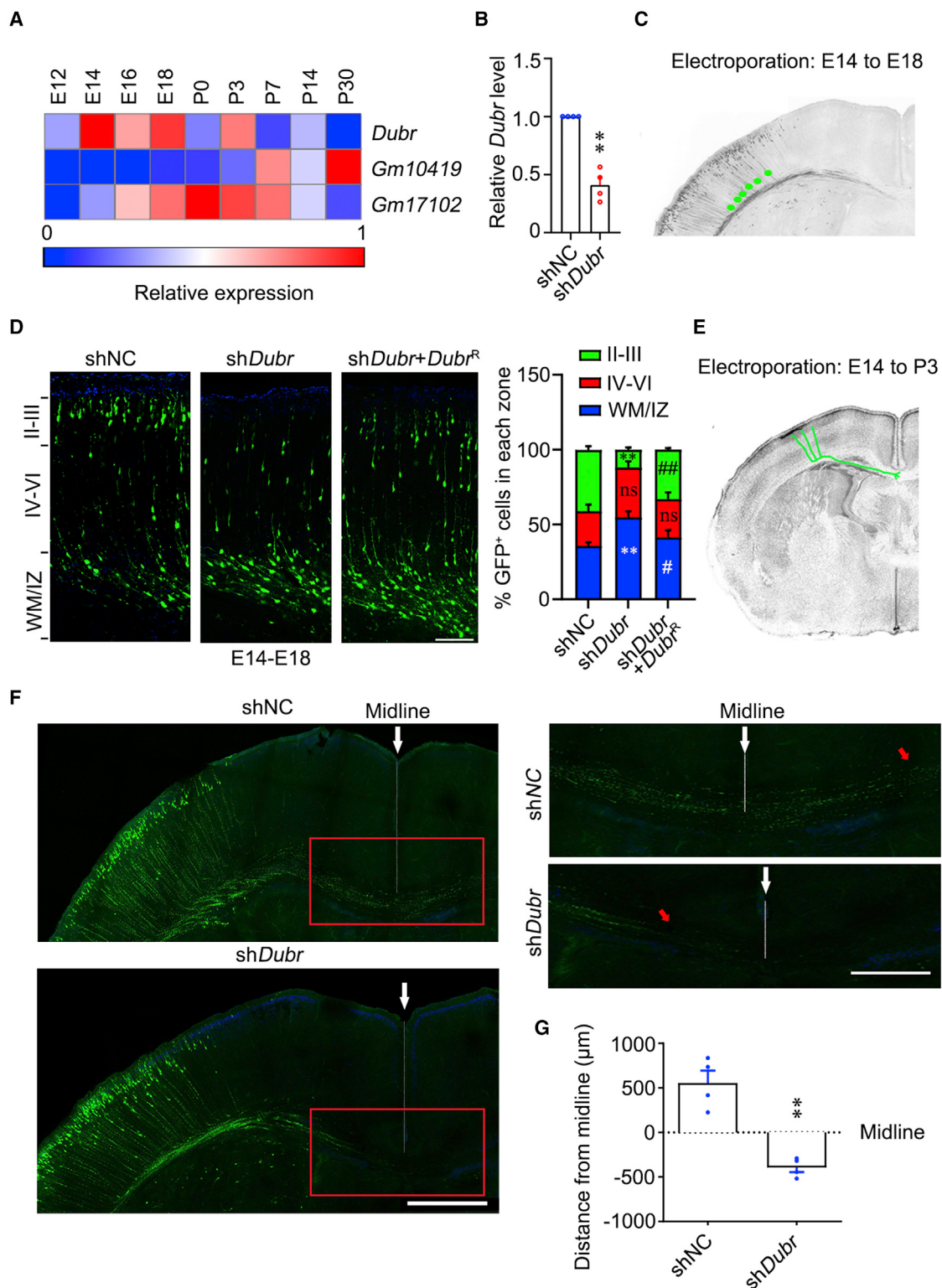


Figure 3. Downregulation of *Dubr* causes delayed radial migration and axon projection of cortical neurons

(A) Heatmap of RNA-seq from E12 to P30 cortex showed that *Dubr* was highly expressed at E14, E18, and P3. Other lncRNAs such as *Gm10419* and *Gm17102* were abundantly expressed at P30 and P0, respectively. n = 3.

(B) qPCR showed that the expression of *Dubr* was significantly decreased after transfection of sh*Dubr* in cultured P0 cortical neurons. **p < 0.01 versus shNC. n = 4.

(legend continued on next page)

was divided into cortical plate (CP), including layers of II-III and IV-VI, white matter (WM), and ventricular zone (VZ). Importantly, immunofluorescence images showed that knockdown of *Dubr* significantly decreased the percentage of GFP⁺ neurons in layer II-III of the CP and increased the percentage of GFP⁺ neurons in the WM/VZ (Figure 3D). Meanwhile, the defect of neuronal migration caused by sh*Dubr* was largely rescued by coexpression of shRNA-resistant *Dubr* (*Dubr*^R) (Figure 3D), suggesting that the phenotype caused by sh*Dubr* is not an off-target effect. Therefore, downregulation of *Dubr* affects the migration of cortical neurons in the central nerve system.

To further evaluate the effect of *Dubr* during axon development, we examined axon projection of cortical neurons at P3, a critical period for extending their callosal axons across the corpus callosum (Poulopoulos et al., 2019). Immunofluorescence images and quantitative data showed that the callosal axons expressing negative control shRNA (shNC) could mostly cross the midline at P3, whereas the callosal axons expressing sh*Dubr* did not reach the midline (Figures 3E and 3F), suggesting a regulatory role of *Dubr* during the axon projection of cortical neurons. Taken together, these data indicate that downregulation of *Dubr* causes delayed migration and axon projection of cortical neurons.

m⁶A modification of *Dubr* is a requisite for its functions during neuronal development

To explore the role of m⁶A modification on the *Dubr*-mediated functions, we firstly reanalyzed the SMART-seq data by m⁶A-CLIP from mouse DRGs (Weng et al., 2018) and found that the m⁶A peaks were highly enriched in the conserved region of *Dubr* isoforms (Figure 4A). Then, we searched the potential m⁶A-modified sites in the conserved region of *Dubr* according to specific methylation motifs by the complex comprising methyltransferase-like 3 (METTL3) and METTL14 (Li et al., 2019). Four high-confidence m⁶A-modified motifs, including three GGACU and one GGACA, were enriched within the 200-nt length of this conserved region by RNAstructure software (Figure S3A). Meanwhile, these methylated motifs were also observed in lncRNA *H19*. RIP experiments followed by qPCR in DRGs showed that two isoforms of *Dubr*, not for *Ak047676*, were abundantly present in the immunoprecipitates by m⁶A antibody (Figures 4B and S3B). To validate the m⁶A-modified motifs within *Dubr*, we generated the constructs of two isoforms, including wildtype *Dubr* (*Dubr*^{WT}) and mutant *Dubr* (*Dubr*^{Mut}), comprising the mutation of four m⁶A sites, including m⁶A234, m⁶A256, m⁶A376, and m⁶A422 (Figure S3C). RIP experiments followed by qPCR detected that the mutation of four m⁶A sites dramatically reduced the m⁶A-modified levels of two exogenously expressed *Dubr*

isoforms in ND7/23 cells (a hybrid cell line derived from rat DRG neuron fused with mouse neuroblastoma cells), which express a similar level of *Dubr* as cultured P0 DRG neurons (Figure S3D), whereas the methylation of endogenous *H19* was not affected (Figures 4C and S3E). In addition, we carried out the single-base elongation- and ligation-based qPCR amplification method (SELECT) as reported previously (Xiao et al., 2018) to validate the m⁶A-methylated sites of *Dubr*. qPCR showed that fat mass and obesity-associated protein (FTO), an m⁶A demethylase, significantly decreased the level of m⁶A modification on four sites in *Dubr* from the RNA lysates of ND7/23 cells (Figure S3F), suggesting the site specificity of m⁶A modification on *Dubr*. Thus, four motifs in the conserved region of *Dubr* are mainly required for its m⁶A modification.

We further examined the effect of m⁶A modification for *Dubr* on axon elongation in microfluidic-cultured P0 DRG neurons. Although qPCR showed that overexpression of siRNA-resistant *Dubr*^{Mut} (*Dubr*^{MutR}) completely rescued the amounts of *Dubr* in both cell bodies and axons affected by selective knockdown of *Dubr* in cell bodies (Figure S3G) or axons (Figure S3H), the decreased axon elongation by si*Dubr* was not rescued by specific expression of *Dubr*^{MutR} in cell bodies (Figure 4D) or axons (Figure 4E), implying that the m⁶A modification of *Dubr* is indeed required to maintain axon elongation. Moreover, we also evaluated the effect of m⁶A modification for *Dubr* on the radial migration of cortical neurons. Immunofluorescence images and quantitative data showed that coexpression of *Dubr*^{MutR} failed to rescue the decreased percentage of cortical neurons in layer II-III at E18 (Figure 4F), suggesting that the m⁶A modification is crucial for the *Dubr*-mediated regulation of neuronal migration. These results highlight the necessity of m⁶A modification for *Dubr* during neuronal development in both peripheral and central nerve systems.

Dubr interacts with YTHDF1/3 and regulates their protein levels through m⁶A modification

Since the m⁶A modification of *Dubr* played a crucial role in neuronal development, we then explored the underlying mechanism. Given the cytoplasmic localization of *Dubr*, we speculate that *Dubr* may exert its functions by regulating mRNA translation. To investigate whether *Dubr* was possibly involved in mRNA translation, we performed polysome profiling as reported previously (Pan et al., 2021) due to the relatively higher expression of *Dubr* in the cortex of mouse brain at P3 (Figure 3A), which is a critical period of axon projection in cortical neurons (Figure 3F). The polysome profiling chart showed that the ribosome subunits (40s and 60s), and monosome (80s) and polysome fractions, were successfully separated based on the level of ribosomal

(C) A schematic showing the flowchart of *in utero* electroporation in the cerebral cortex of E14 mice. The radial glia progenitors were electroporated with the constructs containing shRNA and GFP reporter. The GFP-positive (GFP⁺) cells were analyzed in the somatosensory cortex at E18.

(D) Representative images (left) and quantitative data (right) showed that knockdown of *Dubr* caused delayed neuronal migration, and coexpression of *Dubr* partially rescued the defects. The percentage of electroporated cells (at least 400 neurons from 3 mice) was calculated in each region, including layers of II-III, IV-VI, and WM/VZ (shNC, n = 5; sh*Dubr*, n = 6; sh*Dubr* + *Dubr*^R, n = 6). **p < 0.01 versus shNC and #p < 0.05, ##p < 0.01 versus sh*Dubr*. ns, non-significant, sh*Dubr* versus shNC or sh*Dubr* + *Dubr*^R, respectively. Scale bar, 300 μm.

(E) A schematic showing the flowchart for detection of the callosal axon projection in corpus callosum. *In utero* electroporation was performed in the cerebral cortex of E14 mice. A coronal section at P3 visual cortex was used to access the axon projections from these neurons expressing GFP.

(F and G) Representative images (F) and quantitative data (G) showed that knockdown of *Dubr* delayed the axon projection of neurons in the somatosensory cortex (n = 4). Arrows indicate midline (white) and the distal axon (red), respectively. Scale bar, 300 μm. **p < 0.01 versus shNC. All results are presented as mean ± SEM.

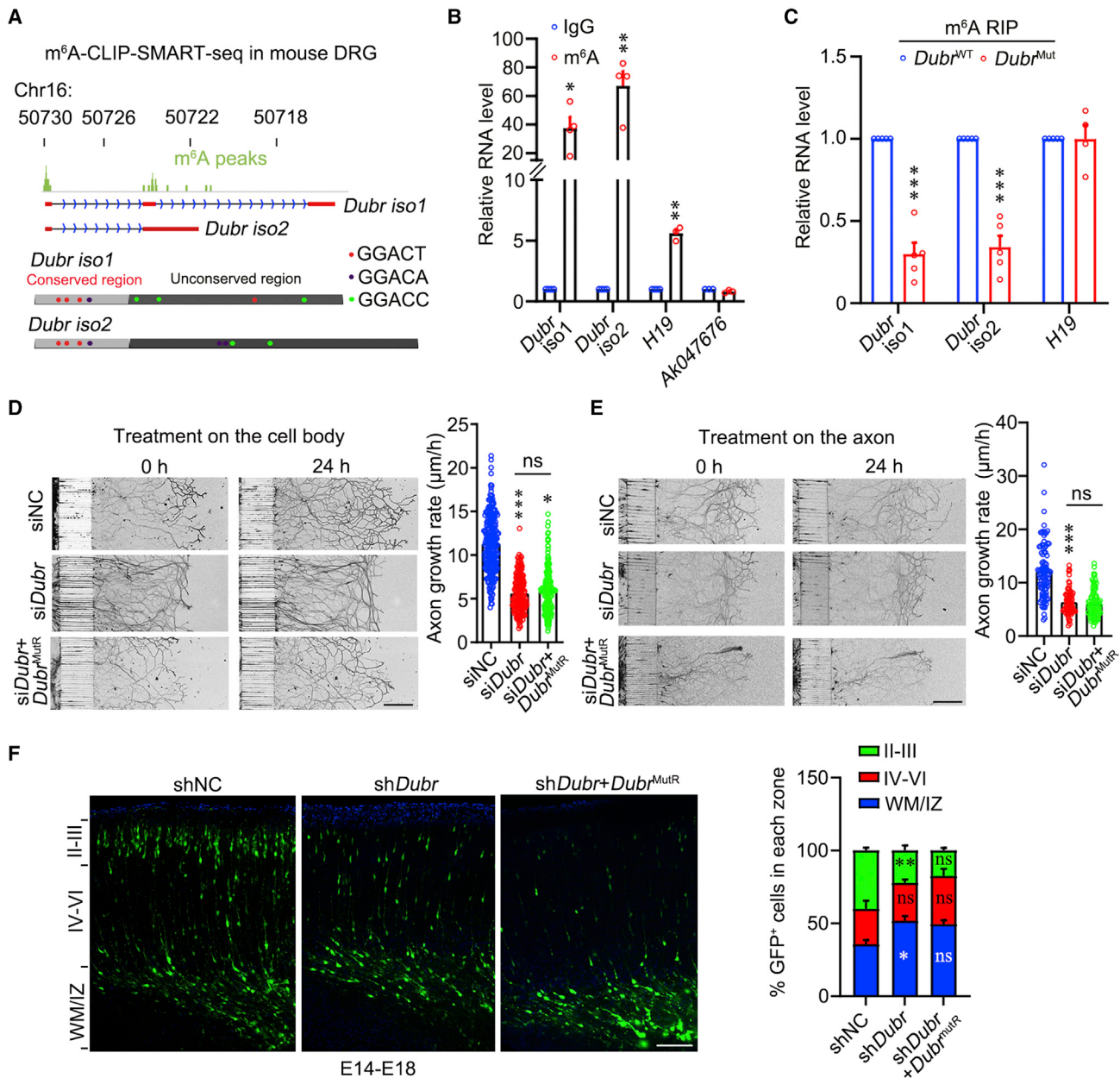


Figure 4. m⁶A modification of Dubr is required for the axon elongation of DRG neurons and the radial migration of cortical neurons

(A) m⁶A-CLIP-SMART-seq coverage showed that the m⁶A peaks were enriched in the conserved region of Dubr. The m⁶A-modified motifs, including three GGACU and one GGACA were enriched within this conserved region.

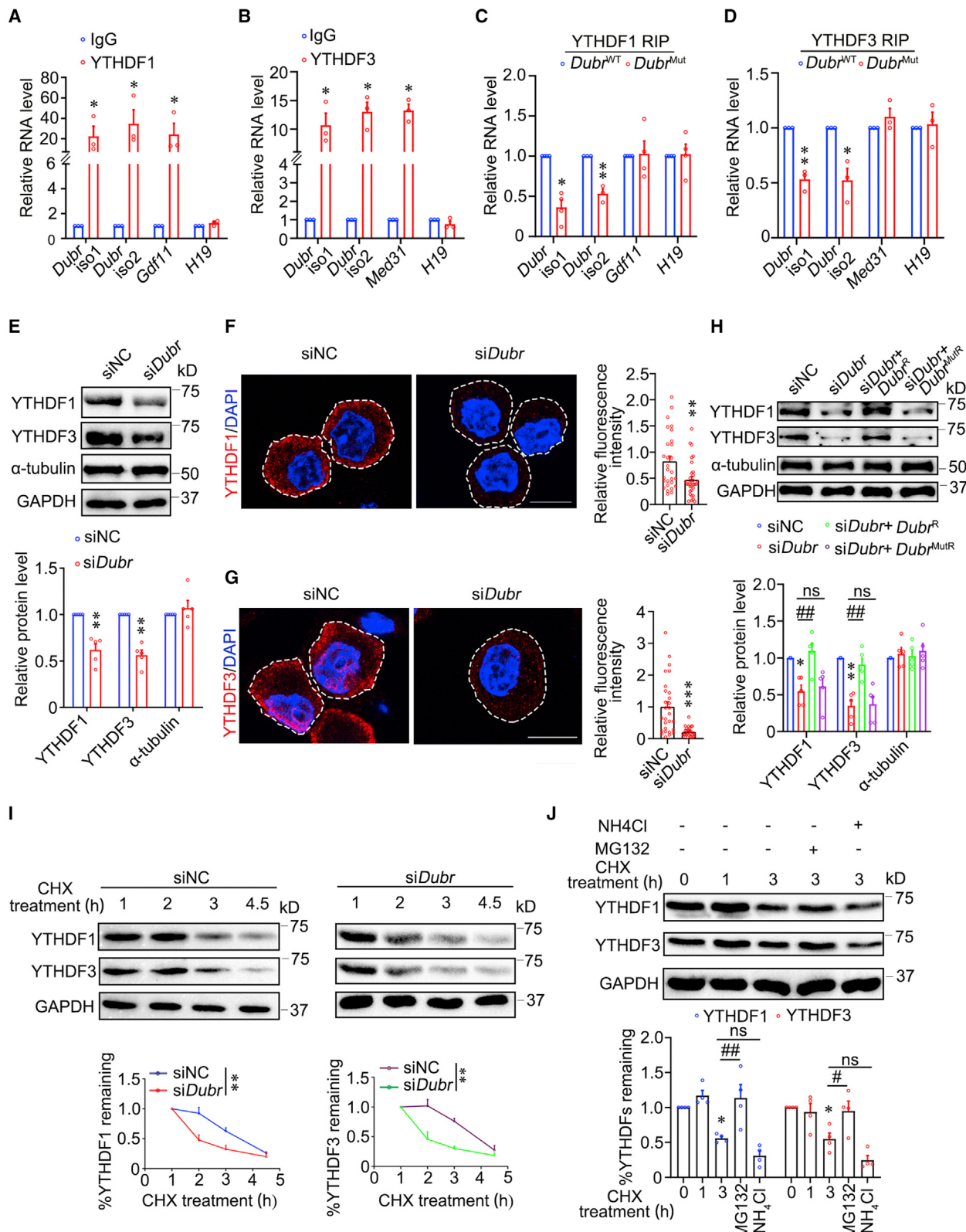
(B) qPCR showed that Dubr iso1 and iso2 were enriched in the m⁶A immunoprecipitates of ND7/23 cells. H19 and Ak047676 served as a positive and negative control, respectively. *p < 0.05, **p < 0.01 versus IgG. n = 4.

(C) qPCR showed that the enrichment of Dubr^{Mut} including iso1 and iso2 were largely reduced in the m⁶A immunoprecipitates of ND7/23 cells. H19 served as a negative control. ***p < 0.001 versus Dubr^{WT}. n = 5.

(D) Representative images (left) and quantitative data (right) showed that the reduced axon elongation induced by siDubr treatment on the cell body was not rescued by coexpression of Dubr^{Mut} in the cell body compartment (siNC, n = 243; siDubr, n = 194; siDubr + Dubr^{MutR}, n = 188). ***p < 0.001 versus siNC. ns, non-significant versus indicated. Scale bar, 300 μm .

(E) Representative images (left) and quantitative data (right) showed that the reduced axon elongation induced by siDubr treatment on the axon was not rescued by coexpression of Dubr^{Mut} in the axon compartment (siNC, n = 97; siDubr, n = 83; siDubr + Dubr^{MutR}, n = 106). ***p < 0.001 versus siNC. ns, non-significant versus indicated. Scale bar, 300 μm .

(F) Representative images (left) and quantitative data (right) showed that the delayed neuronal migration caused by shDubr was not rescued by coexpression of Dubr^{MutR}. The percentage of electroporated cells (at least 400 neurons from 3 mice) was calculated in each region. *p < 0.05, **p < 0.01 versus shNC and ns versus shDubr. ns, non-significant, shDubr versus shNC or shDubr + Dubr^{MutR} in the IV-VI regions, shDubr versus shDubr + Dubr^{MutR} in the WM/Iz regions. Scale bar, 300 μm . n = 4. All results are presented as the mean \pm SEM. See also Figure S3.



(legend on next page)

RNA detected by UV detection at 254 nm in different fractions. Interestingly, qPCR analysis showed that *Dubr* was mainly distributed in the 80s and polyribosome fractions (Figure S4A), which largely overlaps with RPL4, a ribosome protein enriched in the polysome, further indicating a potential role of *Dubr* involvement in the translational regulation of mRNA.

Previous studies have shown that YTH domain family proteins, such as YTHDFs, function as the m⁶A reader by directly binding the m⁶A modification sites of RNAs to mediate their translation and degradation (Huang et al., 2020; Shi et al., 2017; Wang et al., 2015c). To detect whether *Dubr* associates with YTHDFs, we performed RIP experiments in P0 DRGs using antibodies of YTHDF1 and YTHDF3. YTHDF2 plays a role in the decay of m⁶A-modified transcripts (Wang and Lu, 2021), and is not considered for this study. Immunoblotting detected that YTHDF1 and YTHDF3 were successfully pulled down by their antibodies (Figures S4B and S4C). The following qPCR showed that two isoforms of *Dubr* but not *H19* were apparently present in the immunoprecipitates of either YTHDF1 or YTHDF3 in P0 DRGs (Figures 5A and 5B). Other known m⁶A-modified RNAs, *Gdf11* and *Med31*, that have been reported to bind YTHDF1 and YTHDF3, respectively (Weng et al., 2018), were also detected in the corresponding immunoprecipitates of YTHDF1 and YTHDF3 (Figures 5A and 5B). These data suggest the specific association of YTHDFs with *Dubr*.

To further evaluate whether the m⁶A-modified sites were required for *Dubr* to interact with YTHDF1 and YTHDF3, we performed RIP in ND7/23 cells expressing either *Dubr*^{WT} or *Dubr*^{Mut} constructs, which displayed comparable levels of exogenously expressed *Dubr* (Figure S4D). Notably, qPCR following RIP showed that the enrichment of *Dubr* in the immunoprecipitates of YTHDF1 and YTHDF3 in cells expressing *Dubr*^{WT} was dramatically reduced in cells expressing *Dubr*^{Mut} (Figures 5C, 5D, and S4E), suggesting that m⁶A modification for *Dubr* is required for the association with YTHDF1 and YTHDF3. Therefore, *Dubr* interacts with YTHDFs mainly by its m⁶A modification.

Given the known function of YTHDF1 in axon guidance (Zhuang et al., 2019), we speculate that *Dubr* may exert its functions by affecting YTHDFs. As expected, immunoblotting showed that knockdown of *Dubr* significantly reduced the protein levels of YTHDF1 and YTHDF3 in cultured P0 DRG neurons (Figure 5E). Meanwhile, immunofluorescence images and quan-

titative data also showed that knockdown of *Dubr* decreased the intensity of YTHDF1 and YTHDF3 in the cell bodies of cultured P0 DRG neurons (Figures 5F and 5G). Furthermore, coexpression of *Dubr*^R fully rescued the decreased protein levels of YTHDF1 and YTHDF3 due to si*Dubr* in cultured P0 DRG neurons, suggesting that the *Dubr*-mediated regulation is not an off-target effect (Figure 5H). Importantly, coexpression of *Dubr*^{MutR} failed to rescue the si*Dubr*-mediated downregulation of YTHDF1 and YTHDF3 (Figure 5H). These data suggest that *Dubr* is required for maintaining the protein levels of YTHDF1 and YTHDF3 through its m⁶A modification.

Interestingly, the mRNA levels of *Ythdf1* and *Ythdf3* were not affected by si*Dubr* (Figure S4F), raising the possibility of *Dubr* regulation in the protein stability of YTHDFs. To evaluate the effect of *Dubr* on the stability of YTHDFs, we performed cycloheximide (CHX) chase assay in ND7/23 cells. Immunoblotting showed that YTHDF1 and YTHDF3 were gradually decreased in the presence of CHX (60 µg/mL) (Figure 5I), whereas knockdown of *Dubr* significantly accelerated this process (Figure 5I), implying the *Dubr*-mediated stabilization of YTHDFs. Moreover, treatment with a proteasome inhibitor of MG132 (10 µM) was able to fully prevent the decreased protein levels of YTHDF1 and YTHDF3 by si*Dubr* in the presence of CHX for 3 h, but not application with a lysosomal protein degradation inhibitor of NH₄Cl (25 µM) (Figure 5J), suggesting that *Dubr* regulates the stability of YTHDFs via the proteasome pathway. These data suggest that *Dubr* prevents YTHDF1/3 from degradation via the proteasome pathway.

Both *Dubr* and YTHDF1/3 regulate the translation of *Tau* and *Calmodulin* in DRG neurons

YTHDF1/3 are previously shown as readers to recognize m⁶A-modified transcripts and orchestrate their translation in distinct biological processes (Shi et al., 2017; Wang et al., 2015c; Yu et al., 2018). To explore the possible downstream targets of YTHDFs in DRG neurons, we obtained YTHDF-associated genes and the axonal transcriptome of embryonic DRG neurons (Gumy et al., 2011; Wang et al., 2015c), and subsequently analyzed the overlapping molecules. A total of 569 transcripts were identified as YTHDF-associated genes in DRG neurons. Then, we utilized gene ontology (GO) analysis to evaluate the potential functions of these genes, and found those genes highly enriched in

Figure 5. *Dubr* interacts with YTHDF1/3 and regulates their protein levels through m⁶A modification

(A and B) qPCR showed that *Dubr* iso1 and iso2 were highly abundant in the immunoprecipitates of YTHDF1 (A) and YTHDF3 (B) in ND7/23 cells, respectively. IgG served as a control. *H19* was indicated as a negative control. *p < 0.05 versus IgG. n = 3.

(C and D) qPCR showed that the enrichment of *Dubr*^{Mut}, including iso1 and iso2, were largely reduced in the YTHDF1 (C) (n = 4) or YTHDF3 (D) (n = 3) immunoprecipitates of ND7/23 cells (n = 4). *Gdf11*, *Med31*, and *H19* served as negative controls. *p < 0.05, **p < 0.01 versus *Dubr*^{WT}.

(E) Representative immunoblots and quantitative data (down) showed that application of si*Dubr* decreased the protein levels of YTHDF1 and YTHDF3, respectively. GAPDH served as a loading control. **p < 0.01 versus siNC. n = 5.

(F and G) Representative images and quantitative data showed that knockdown of *Dubr* decreased the intensity of YTHDF1 (E) (n = 28) and YTHDF3 (F) (n = 28) in cultured P0 DRG neurons. **p < 0.01, ***p < 0.001 versus siNC.

(H) Representative immunoblots and quantitative data (down) showed that the decreased protein level of YTHDF1 and YTHDF3 due to si*Dubr* was fully restored by coexpression of *Dubr*^R but not *Dubr*^{MutR}. GAPDH and α-tubulin served as a loading control and negative control, respectively. *p < 0.05, **p < 0.01 versus siNC, and #p < 0.05, ns versus indicated. n = 5.

(I) Representative immunoblots (left) and quantitative analysis (right) showed that application of si*Dubr* accelerated the protein degradation rate of YTHDF1 and YTHDF3, respectively. GAPDH served as a loading control. **p < 0.01 versus siNC by two-way ANOVA test. n = 4.

(J) Representative immunoblots and quantitative data (down) showed that MG132, not for NH₄Cl could fully block the protein degradation of YTHDF1 and YTHDF3 (n = 4), respectively. *p < 0.05 versus 0 h and #p < 0.05, ##p < 0.01, ns versus indicated. All results are presented as the mean ± SEM. See also Figure S4.

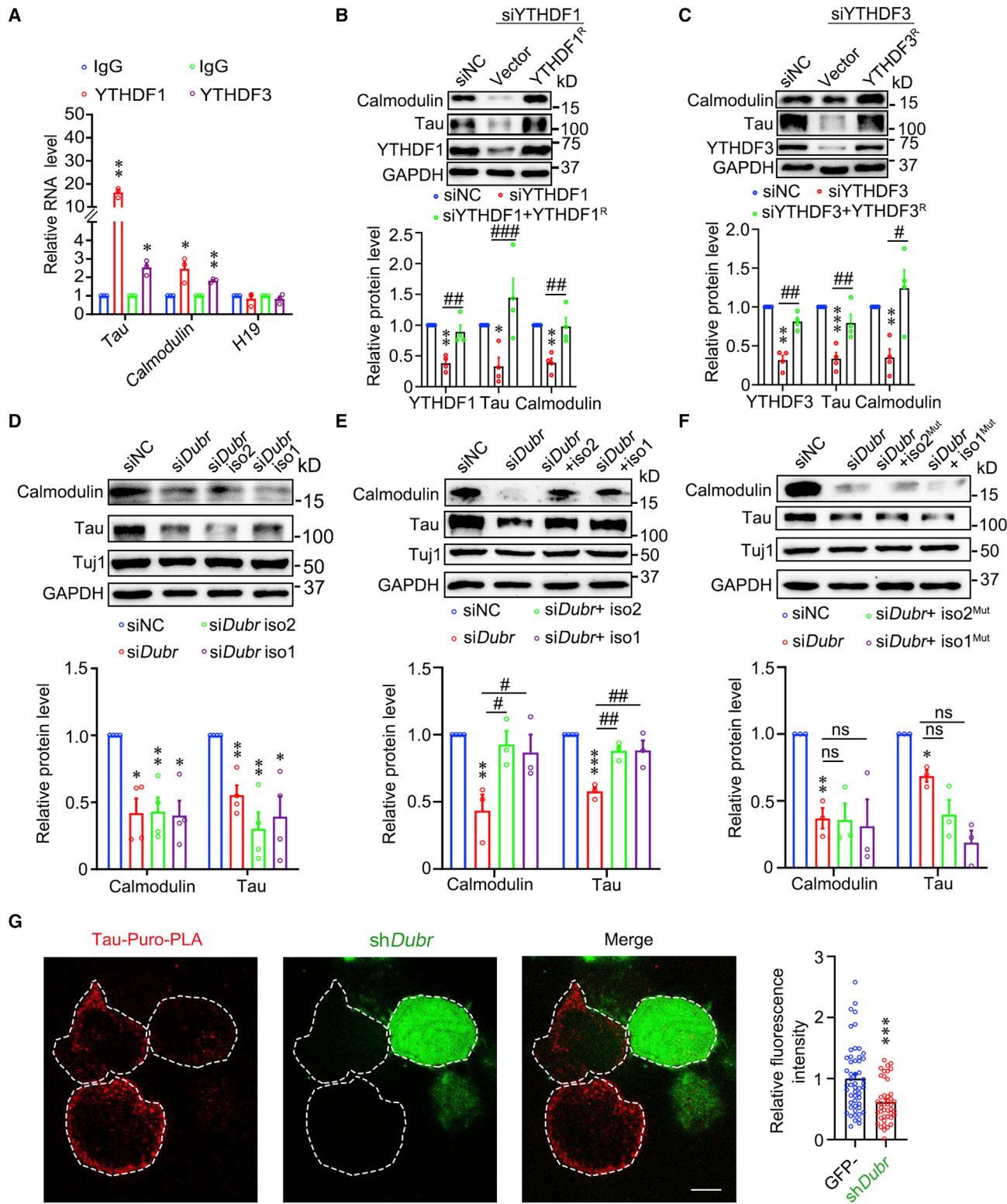


Figure 6. YTHDF1/3 and Dubr regulates the mRNA translation of Tau and Calmodulin

(A) qPCR showed that *Tau* and *Calmodulin* mRNAs were highly abundant in the YTHDF1 and YTHDF3 immunoprecipitates of ND7/23 cells, respectively. IgG served as a control. *H19* was indicated as a negative control. *p < 0.05, **p < 0.01 versus IgG. n = 3.

(legend continued on next page)

cytoskeletal microtubule organization and epidermal growth factor signaling, such as *Tau* and *Calmodulin* (Figure S5A), which have also been reported to be key regulators during neuronal development (Horigane et al., 2019; Takei et al., 2000). Afterward, we examined the association of YTHDF1 and YTHDF3 with *Tau* and *Calmodulin* mRNA. qPCR following RIP showed that the mRNA levels of *Tau* and *Calmodulin* were enriched in the YTHDF1 and YTHDF3 immunoprecipitates of ND7/23 cells (Figure 6A), respectively, suggesting an association of YTHDF1 with *Tau* and *Calmodulin* mRNA.

To determine the effects of YTHDF1 on *Tau* and *Calmodulin*, we detected their protein levels after application of siYTHDF1 and siYTHDF3 in cultured P0 DRG neurons, respectively. Immunoblotting showed that the protein levels of *Tau* and *Calmodulin* were dramatically decreased after knockdown of either YTHDF1 or YTHDF3, while coexpression of siRNA-resistant YTHDF1 (YTHDF1^R) or YTHDF3 (YTHDF3^R) fully rescued the decreased levels of *Tau* and *Calmodulin*, respectively (Figures 6B and 6C), indicating that the defect caused by siYTHDF1 or siYTHDF3 was not due to an off-target effect. To further evaluate the specificity of YTHDF1/3 on *Tau* and *Calmodulin*, we chose calmodulin-regulated spectrin-associated protein family protein 2 (CAMSAP2), which is essential for neuronal development by stabilizing microtubules (Yau et al., 2014), as another candidate from the top GO term. Immunoblotting showed that knockdown of YTHDF3 did not affect the protein level of CAMSAP2 in cultured P0 DRG neurons (Figure S5B), indicating a specific regulation of *Dubr* on *Tau* and *Calmodulin*. In addition, application of siYTHDF1 also greatly reduced the protein level of YTHDF3, whereas application of siYTHDF3 did not affect the level of YTHDF1 (Figure S5C), implying that YTHDF1 orchestrates the expression of YTHDF3. Therefore, YTHDF1/3 regulate *Tau* and *Calmodulin* in DRG neurons.

To examine the effects of *Dubr* on *Tau* and *Calmodulin*, we detected their protein levels by transfecting siRNA to knockdown *Dubr* in cultured P0 DRG neurons (Figure S5B). Immunoblotting showed that silencing either total or each isoform of *Dubr* significantly reduced the protein levels of *Tau* and *Calmodulin* without affecting their mRNA levels (Figures 6D and S5D). Coexpression of *Dubr* isoform 1 or 2 could fully rescue the decreased protein levels of *Tau* and *Calmodulin* due to si*Dubr* treatment (Figures 6E and S5E), whereas coexpression of mutant *Dubr* isoform 1 or 2 failed to restore the phenotypes (Figures 6F, S5F, and S5G), highlighting an importance of m⁶A modification in the *Dubr*-mediated regulation of *Tau* and *Calmodulin*. To examine

whether *Dubr* affects mRNA translation, we performed RIP by antibody of RPL4 in cultured ND7/23 cells. qPCR results showed that the levels of *Tau* and *Calmodulin* were significantly decreased in RPL4 immunoprecipitates after application of si-*Dubr* (Figure S5H), indicating the important role of *Dubr* on the translational regulation. Meanwhile, we detected the translation of *Tau* mRNA by utilizing a puromycin proximity ligation assay (puro-PLA) in cultured P0 DRG neurons. Immunofluorescence images and quantitative data showed that the nascent *Tau* labeling with puro-PLA in neurons expressing sh*Dubr* was dramatically decreased compared with that in those neurons expressing shNC (Figure 6G), suggesting a translational suppression of *Dubr* for *Tau* mRNA. These data suggest that *Dubr* is required for the translational regulation of *Tau* and *Calmodulin* in DRG neurons.

***Dubr* facilitates the YTHDF1/3 complex and its mediated mRNA translation, neuronal migration, and axon elongation**

We explored the role of *Dubr* in YTHDF1/3-mediated function. Previous studies have reported that multivalent m⁶A-containing RNAs facilitate the phase separation of YTHDFs (Ries et al., 2019). To realize whether *Dubr* is coexpressed with YTHDF1 and YTHDF3 in neurons, we reanalyzed the published database of scRNA-seq for the developing mouse cortical neurons (Di Bella et al., 2021) and DRG neurons (Wang et al., 2021a). ScRNA-seq analysis showed that *Dubr*, *Ythdf1*, and *Ythdf3* were mainly coexpressed in the types of apical and intermediate progenitors as well as migrating and mature neurons from embryonic mouse brain cortex (Figure S6A) and almost all types of DRG neurons (Figure S6B), implying a functional cooperation among *Dubr*, YTHDF1, and YTHDF3 during the development of cortical and DRG neurons. Then, we performed RIP to examine the possible role of *Dubr* in the interaction between YTHDF1 and YTHDF3 in cultured ND7/23 cells. Importantly, immunoblotting showed that knockdown of *Dubr* greatly reduced the protein level of YTHDF3 in the YTHDF1 immunoprecipitates of ND7/23 cells (Figure 7A). Meanwhile, overexpression of *Dubr*^{WT}, but not *Dubr*^{MutR}, could rescue the decreased protein level of YTHDF3 in the YTHDF1 immunoprecipitates (Figures 7B and 7C). These data support a crucial role of m⁶A-modified *Dubr* in the formation and stabilization of the YTHDF1-YTHDF3 complex.

To finally validate the effects of YTHDF1/3 on the *Dubr*-mediated functions, we detected the protein levels of *Calmodulin* and *Tau* in cultured P0 DRG neurons coexpressing si*Dubr* with

(B and C) Representative immunoblots (up) and quantitative data (right) showed that coexpression of YTHDF1^R (B) and YTHDF3^R (C) largely rescued the decreased protein level of *Tau* and *Calmodulin* due to siYTHDF1 and siYTHDF3, respectively. GAPDH served as a loading control and negative control, respectively. *p < 0.05, **p < 0.01, ***p < 0.001 versus siNC and #p < 0.05, ##p < 0.01, ###p < 0.001 versus indicated. n = 4.

(D) Representative immunoblots (up) and quantitative data (down) showed that downregulation of either total or each isoform of *Dubr* decreased the protein level of *Tau* and *Calmodulin* in ND7/23 cells. GAPDH and Tuj-1 served as a loading control and negative control, respectively. *p < 0.05 versus siNC. n = 4.

(E) Representative immunoblots (up) and quantitative data (down) showed that coexpression of *Dubr* isoforms rescued the decreased protein level of *Tau* and *Calmodulin* due to si*Dubr*. GAPDH and Tuj-1 served as a loading control and negative control, respectively. **p < 0.01, ***p < 0.001 versus siNC and #p < 0.05, ##p < 0.01 versus indicated. n = 3.

(F) Representative immunoblots (up) and quantitative data (down) showed that coexpression of *Dubr*^{Mut} isoforms failed to rescue the decreased protein level of *Tau* (n = 3) and *Calmodulin* caused by si*Dubr*. GAPDH and Tuj-1 served as a loading control and negative control, respectively. *p < 0.05, **p < 0.01 versus siNC. ns, non-significant.

(G) Representative images (left) and quantitative data (right) showed that knockdown of *Dubr* decreased the newly synthesized *Tau* (red) in cultured P0 DRG neurons (GFP⁻, n = 52; sh*Dubr*, n = 43). ***p < 0.001 versus GFP-negative neurons. All results are presented as the mean ± SEM. See also Figure S5.

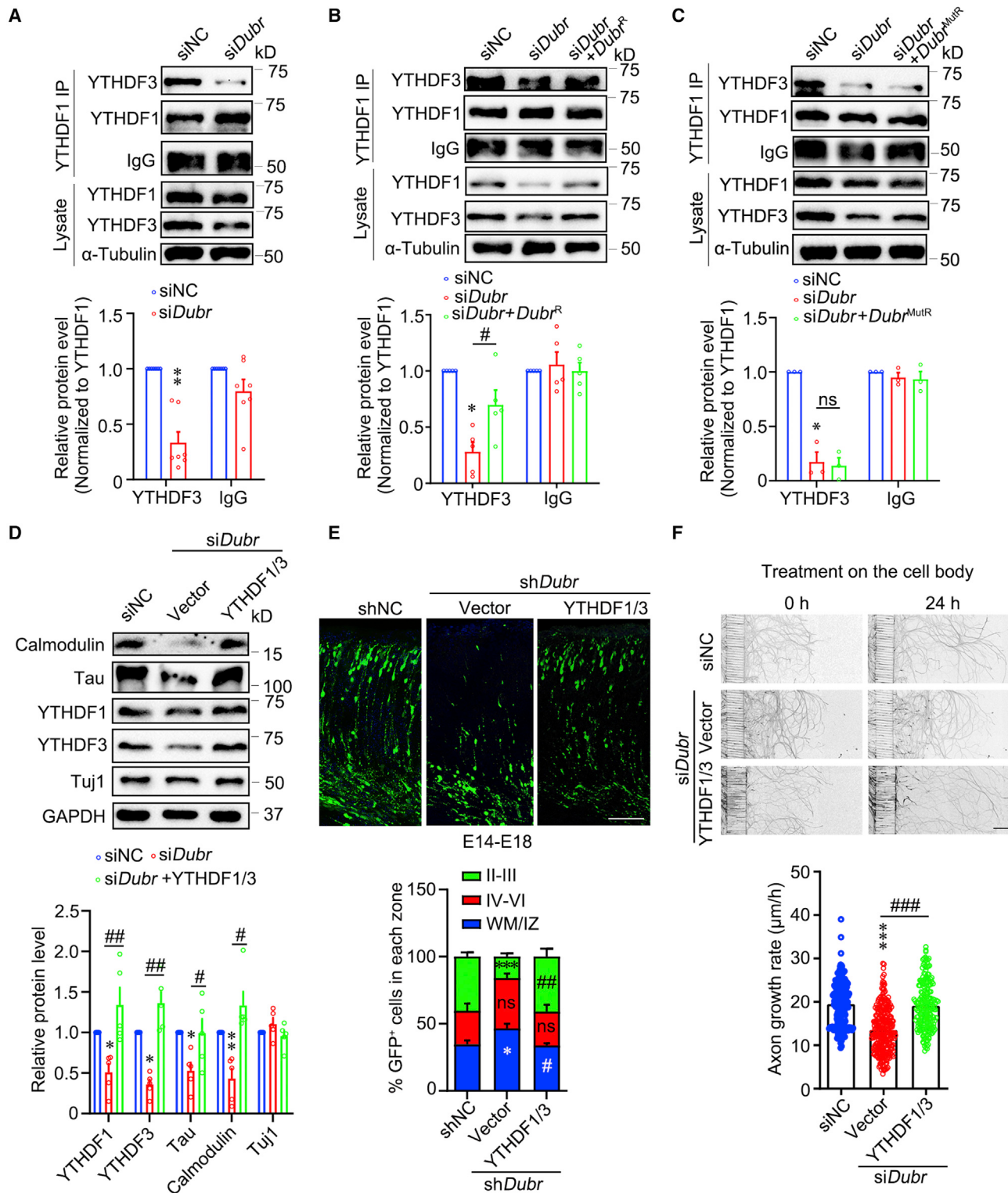


Figure 7. m^6A modification of *Dubr* facilitates YTHDF1/3 complex, mRNA translation of *Tau* and *Calmodulin*, neuronal migration, and axon elongation

(A) Representative immunoblots (up) and quantitative data (down) showed that downregulation of *Dubr* decreased the amount of YTHDF3 in YTHDF1 immunoprecipitates of ND7/23 cells. IgG and α -tubulin served as a negative control and loading control, respectively. n = 7.

(legend continued on next page)

YTHDF1/3. Immunoblotting showed that overexpression of YTHDF1/3 could completely rescue the decreased levels of Calmodulin and Tau due to *siDubr* treatment (Figure 7D), implying an importance of the YTHDF1/3 complex in the downstream *Dubr* effect. At the same time, coexpression of YTHDF1/3 completely rescued the defects of neuronal migration (Figure 7E) and decreased axon elongation (Figure 7F) caused by downregulation of *Dubr*, respectively, further suggesting the crucial role of the YTHDF1/3 complex in *Dubr*-mediated neuronal development. Taken together, *Dubr* functions in neuronal development by facilitating the YTHDF1/3 complex.

DISCUSSION

The m⁶A modification of RNAs has been shown to play crucial roles in neuronal development (Yoon et al., 2017; Yu et al., 2018). In this study, we identified critical roles and underlying mechanisms of m⁶A-modified lncRNA *Dubr* in neuronal development. Normally, *Dubr* interacts and stabilizes YTHDF1/3 through its m⁶A modification, thereby facilitating the translation of Tau and Calmodulin as well as maintaining subsequent axon elongation and neuronal migration. When *Dubr* is downregulated during development, YTHDF1/3 are degraded via the proteasome pathway, and the synthesis of Tau and Calmodulin is simultaneously repressed, thus inhibiting axon elongation and neuronal migration (Figure S7). Our study uncovers the regulatory effect of m⁶A-modified lncRNA during the development of the nervous system.

m⁶A-modified and neuron-enriched *Dubr* promotes neuronal development

Accumulated evidence reveals that the m⁶A modification of mRNAs is highly enriched in the developing nervous system (Widagdo and Anggono, 2018). Despite hundreds of m⁶A-modified mRNAs having been identified to play divergent roles in neurogenesis and synaptic transmission (Shi et al., 2018; Widagdo and Anggono, 2018; Zhuang et al., 2019), direct evidence in regard to the function of methylated lncRNAs has yet to be reported during the development of the nervous system. To determine the m⁶A-modified lncRNAs, we reanalyzed previously reported SMART-seq data by m⁶A-CLIP from mouse DRGs. Among those methylated lncRNAs, we identified a neuron-enriched lncRNA *Dubr*, which was highly expressed during the early-stage development of DRGs and cerebral cortex. In addition, we also found that other methylated lncRNA *Gm12371* was highly expressed at the postnatal stage of

DRGs. *Gm12371* has been shown to regulate the expression of several neuronal development-related genes and synapse formation in hippocampal neurons (Raveendra et al., 2018), implying a possible role for m⁶A modification for lncRNAs during different developing stages of neurons. The functions and related mechanisms of other methylated lncRNAs require further investigation.

As an early-stage expressed and neuron-enriched lncRNA, we picked up *Dubr* to determine its roles in neuronal development. Despite *Dubr* (also called *Dum*) having been reported previously to promote muscle cell differentiation and muscle regeneration (Wang et al., 2015b), the regulatory effect of *Dubr* during the development of the nervous system has not been explored. In the present study, downregulation of *Dubr* in ex-vivo-cultured P0 DRG explants and microfluidic-cultured P0 DRG neurons significantly suppressed axon elongation, highlighting a crucial role of *Dubr* in axon development. On the other hand, given the spatially temporal expression of *Dubr* in the intermediate progenitor cells of mouse cortex at E14, knockdown of *Dubr* resulted in the delayed migration of cortical neurons and subsequent axon projection, emphasizing a broader role of *Dubr* during the development of the peripheral and central nervous systems.

Notably, in the present study, loss of m⁶A modification for *Dubr* almost impaired its functions in axon elongation and neuronal migration, imposing an importance of m⁶A modification as a molecular switch in lncRNA-exerted effects. Interestingly, recent studies revealed that two well-known lncRNAs, *Malat1* and *Neat1*, exert their actions mainly by m⁶A modification during the development of metastasis (Wang et al., 2021c; Wen et al., 2020), suggesting a universal role of m⁶A modification for lncRNAs in distinct cell contexts. More importantly, the enrichment of m⁶A-modified motifs within the conserved region of *Dubr* isoforms may be largely crucial for recruiting distinct m⁶A-binding proteins as reported recently (Gao et al., 2019; Wang et al., 2021c), highlighting the key effects of m⁶A modification on individual lncRNA.

m⁶A-modified *Dubr* stabilizes YTHDF1/3 and thereby facilitates mRNA translation of tau and calmodulin

As m⁶A readers, YTHDFs directly recognize and bind the m⁶A-modified mRNAs to regulate their translation or degradation (Yu et al., 2018; Zhuang et al., 2019). Although previous studies report that YTHDFs exhibit the functions during development of nervous system, such as axon guidance (YTHDF1) and synapse formation (YTHDF1 and YTHDF3), the regulation of YTHDFs

(B and C) Representative immunoblots (up) and quantitative data (down) showed that the decreased YTHDF3 in YTHDF1 immunoprecipitates caused by *siDubr* was partially rescued by coexpressed *Dubr*^{WT} (B), but not *Dubr*^{MutR} in ND7/23 cells. IgG and α -tubulin served as a negative control and loading control, respectively. n = 5. The original intensities of immunoblots for YTHDF3 and IgG were normalized by immunoprecipitated YTHDF1. The y axis represents the relative YTHDF3 pulled down by YTHDF1 versus the siNC group.

(D) Representative immunoblots (up) and quantitative data (down) showed that coexpression of YTHDF1/3 fully rescued the decreased protein level of Tau and Calmodulin caused by *siDubr*. GAPDH and Tuj-1 served as a loading control and negative control, respectively. n = 5.

(E) Representative images (up) and quantitative data (down) showed that the delayed neuronal migration caused by sh*Dubr* was completely rescued by co-expression of YTHDF1/3. The percentage of electroporated cells (at least 400 neurons from 3 mice) was calculated in each region (shNC, n = 4; sh*Dubr*, n = 4; sh*Dubr* + YTHDF1/3, n = 3). *p < 0.05, **p < 0.001 versus shNC and #p < 0.05, ##p < 0.01 versus sh*Dubr*. ns versus sh*Dubr*. Scale bar, 300 μ m.

(F) Representative images (up) and quantitative data (down) showed that the reduced axon elongation due to *siDubr* in the cell body compartment was completely restored by coexpression of YTHDF1/3 in cell bodies (siNC, n = 203; *siDubr*, n = 281; *siDubr* + YTHDF1/3, n = 216). ***p < 0.001 versus siNC and ###p < 0.001 versus *siDubr*. Scale bar, 300 μ m. All results are presented as the mean \pm SEM. See also Figures S6 and S7.

themselves by lncRNAs remains unclear. In this study, *Dubr* was detected by RIP to associate with YTHDF1/3 especially through its m⁶A modification sites. In addition, puro-PLA and RPL4 RIP experiments showed that knockdown of *Dubr* decreased the mRNA translation of Tau and Calmodulin (Figures 6G and S5H), suggesting that *Dubr* likely cooperates with YTHDF1/3 in regulating mRNA translation, but not with YTHDF2 in affecting mRNA degradation. More importantly, knockdown of *Dubr* led to the rapid turnover of YTHDF1/3, similar to a previous report that lncRNA *PVT1* interacted with MYC protein and prevented its degradation in cancer cells (Tseng et al., 2014). These studies imply a mechanism of lncRNA-mediated protein stabilization in cells. A recent study reveals that lncRNA *Fendrr* protects NLR-family CARD-containing protein 4 from degradation by inhibiting its ubiquitination (Wang et al., 2021b). The precise mechanism for the *Dubr*-mediated degradation of YTHDF1/3 requires future investigation.

Neuronal migration and axon elongation are critical events in neuronal development for the proper construction of brain architecture (Poulopoulos et al., 2019; Wu et al., 2013). Intracellular calcium signaling especially for the calcium sensor protein, Calmodulin, has been identified to regulate neuronal migration of cerebral cortex (Horigane et al., 2019) and axon elongation of DRG neurons (Wang et al., 2015a). On the other hand, Tau is a well-known microtubule-associated protein for maintaining neuronal development, such as neuronal migration and axon growth (Takei et al., 2000). Given the joint effects of Tau and Calmodulin in axon elongation and neuronal migration, the effective action of *Dubr* in neuronal development could be well explained in both peripheral and central nervous systems. Despite the fact that Tau and Calmodulin were listed within m⁶A-modified mRNAs according to the SMART-seq data by m⁶A-CLIP, the m⁶A-mediated regulation of Tau and Calmodulin has not been explored during neuronal development. This study detected the association of YTHDF1/3 with *Tau* and *Calmodulin* mRNAs. Meanwhile, downregulation of YTHDF1/3 dramatically reduced the protein levels of Tau and Calmodulin, similar to the effects of *Dubr* knockdown, implying the possibility of m⁶A modification in the translational regulation of Tau and Calmodulin. Moreover, coexpression of YTHDF1/3 restored the decreased protein levels of Tau and Calmodulin by si*Dubr* treatment in DRG neurons, implicating the importance of coordinate regulation of the YTHDF1/3 complex in the *Dubr*-mediated effects. Interestingly, our previous study revealed that the translation of Calmodulin is repressed by axon-enriched miR-181d (Wang et al., 2015a), suggesting the intricate coordinated regulation of a protein translation in neurons by distinct ways. In addition, RIP followed by qPCR analysis showed that *Ythdf3* mRNA is associated with YTHDF1 (unpublished data), implying a possible role for YTHDF1 in regulating YTHDF3 translation. The precise mechanism for YTHDF1-mediated regulation of YTHDF3 requires further investigation.

LIMITATIONS OF THE STUDY

The limitation in this study is that m⁶A-modified lncRNAs are analyzed from the m⁶A-CLIP-seq database at adult DRG, more m⁶A-enriched lncRNAs at early-stage development of brain

can be profiled in further analysis. In addition, although our study shows that *Dubr* affects the stability of YTHDF1/3, we cannot address whether *Dubr* directly regulates YTHDF3 since downregulating YTHDF1 also reduces the expression of YTHDF3. Furthermore, the association and precise mechanisms of *Dubr* with other cytoplasmic m⁶A reader proteins in regulating mRNA translation require further investigation.

STAR★METHODS

Detailed methods are provided in the online version of this paper and include the following:

- **KEY RESOURCES TABLE**
- **RESOURCE AVAILABILITY**
 - Lead contact
 - Materials availability
 - Data and code availability
- **EXPERIMENTAL MODEL AND SUBJECT DETAILS**
 - Animals
 - Cell lines
 - Primary culture of DRG explants and neurons
- **METHOD DETAILS**
 - Plasmids
 - Cell transfection
 - RNA extraction, RT-PCR and qPCR
 - Immunostaining
 - Immunoblotting
 - *In situ* hybridization
 - Axon elongation assay
 - *In utero* electroporation
 - Immunoprecipitation and RNA immunoprecipitation (RIP)
 - The SELECT detection assay
 - Detection of protein stability
 - Puromycylation-PLA assay
- **QUANTIFICATION AND STATISTICAL ANALYSIS**
 - Analysis of m⁶A-modified RNAs in the DRG of adult mice
 - Statistical analysis

SUPPLEMENTAL INFORMATION

Supplemental information can be found online at <https://doi.org/10.1016/j.celrep.2022.111693>.

ACKNOWLEDGMENTS

This work was supported by grants from National Natural Science Foundation of China (32070967 and 32070968) and Guangdong High Level Innovation Research Institute (2021B0909050004).

AUTHOR CONTRIBUTIONS

J.S.H. performed the majority of the experiments and analyzed the data. B.W.J. performed the PLA experiments with M.W. G.-W.L. analyzed the RNA-seq data supervised by L.Y. M.L., and D.Z., and X.X. performed the IUE experiments and analyzed data. X.P. helped plasmid construction and qPCR. X.L. made microfluidic devices instructed by X.J. X.Z. instructed some experiments. B.W., L.B., and J.S.H. designed the research and wrote the manuscript.

DECLARATION OF INTERESTS

The authors declare no competing interests.

INCLUSION AND DIVERSITY

We support inclusive, diverse, and equitable conduct of research.

Received: October 27, 2021

Revised: September 16, 2022

Accepted: October 31, 2022

Published: November 22, 2022

REFERENCES

- Aprea, J., Prenninger, S., Dori, M., Ghosh, T., Monasor, L.S., Wessendorf, E., Zocher, S., Massalini, S., Alexopoulou, D., Lesche, M., et al. (2013). Transcriptome sequencing during mouse brain development identifies long non-coding RNAs functionally involved in neurogenic commitment. *EMBO J.* 32, 3145–3160.
- Briggs, J.A., Wolvetang, E.J., Mattick, J.S., Rinn, J.L., and Barry, G. (2015). Mechanisms of long non-coding RNAs in mammalian nervous system development, plasticity, disease, and evolution. *Neuron* 88, 861–877.
- Costa, F.F. (2010). Non-coding RNAs: meet thy masters. *BioEssays. Bio-essays* 32, 599–608.
- Desrosiers, R., Friderici, K., and Rottman, F. (1974). Identification of methylated nucleosides in messenger RNA from Novikoff hepatoma cells. *Proc. Natl. Acad. Sci. USA* 71, 3971–3975.
- Di Bella, D.J., Habibi, E., Stickels, R.R., Scalia, G., Brown, J., Yadollahpour, P., Yang, S.M., Abbate, C., Biancalani, T., Macosko, E.Z., et al. (2021). Molecular logic of cellular diversification in the mouse cerebral cortex. *Nature* 595, 554–559.
- Elsen, G.E., Bedogni, F., Hodge, R.D., Bammler, T.K., MacDonald, J.W., Lindtner, S., Rubenstein, J.L.R., and Hevner, R.F. (2018). The epigenetic factor landscape of developing neocortex is regulated by transcription factors Pax6→Tbr2→Tbr1. *Front. Neurosci.* 12, 571.
- Fu, Y., Dominissini, D., Rechavi, G., and He, C. (2014). Gene expression regulation mediated through reversible m(6)A RNA methylation. *Nat. Rev. Genet.* 15, 293–306.
- Gao, Y., Pei, G., Li, D., Li, R., Shao, Y., Zhang, Q.C., and Li, P. (2019). Multivalent m(6)A motifs promote phase separation of YTHDF proteins. *Cell Res.* 29, 767–769.
- Gumy, L.F., Yeo, G.S.H., Tung, Y.C.L., Zivraj, K.H., Willis, D., Coppola, G., Lam, B.Y.H., Twiss, J.L., Holt, C.E., and Fawcett, J.W. (2011). Transcriptome analysis of embryonic and adult sensory axons reveals changes in mRNA repertoire localization. *RNA* 17, 85–98.
- Guo, Y., Chen, X., Xing, R., Wang, M., Zhu, X., and Guo, W. (2018). Interplay between FMRP and lncRNA TUG1 regulates axonal development through mediating SnoN-Ccd1 pathway. *Hum. Mol. Genet.* 27, 475–485.
- Horigane, S.I., Ozawa, Y., Yamada, H., and Takemoto-Kimura, S. (2019). Calcium signalling: a key regulator of neuronal migration. *J. Biochem.* 165, 401–409.
- Huang, H., Weng, H., Sun, W., Qin, X., Shi, H., Wu, H., Zhao, B.S., Mesquita, A., Liu, C., Yuan, C.L., et al. (2020). Publisher Correction: recognition of RNA N(6)-methyladenosine by IGF2BP proteins enhances mRNA stability and translation. *Nat. Cell Biol.* 22, 1288.
- Kakehi, J., Kawano, E., Yoshimoto, K., Cai, Q., Imai, A., and Takahashi, T. (2015). Mutations in ribosomal proteins, RPL4 and RACK1, suppress the phenotype of a thermospermine-deficient mutant of *Arabidopsis thaliana*. *PLoS One* 10, e0117309.
- Khalil, A.M., Guttman, M., Huarte, M., Garber, M., Raj, A., Rivea Morales, D., Thomas, K., Presser, A., Bernstein, B.E., van Oudenaarden, A., et al. (2009). Many human large intergenic noncoding RNAs associate with chromatin-modifying complexes and affect gene expression. *Proc. Natl. Acad. Sci. USA* 106, 11667–11672.
- Komuro, H., and Rakic, P. (1998). Distinct modes of neuronal migration in different domains of developing cerebellar cortex. *J. Neurosci.* 18, 1478–1490.
- Kosodo, Y., and Huttner, W.B. (2009). Basal process and cell divisions of neural progenitors in the developing brain. *Dev. Growth Differ.* 51, 251–261.
- Kriegstein, A.R., and Noctor, S.C. (2004). Patterns of neuronal migration in the embryonic cortex. *Trends Neurosci.* 27, 392–399.
- Li, L., Wei, D., Wang, Q., Pan, J., Liu, R., Zhang, X., and Bao, L. (2012). MEC-17 deficiency leads to reduced alpha-tubulin acetylation and impaired migration of cortical neurons. *J. Neurosci.* 32, 12673–12683.
- Li, Y., Wu, K., Quan, W., Yu, L., Chen, S., Cheng, C., Wu, Q., Zhao, S., Zhang, Y., and Zhou, L. (2019). The dynamics of FTO binding and demethylation from the m(6)A motifs. *RNA Biol.* 16, 1179–1189.
- Mus, E., Hof, P.R., and Tiedge, H. (2007). Dendritic BC200 RNA in aging and in Alzheimer's disease. *Proc. Natl. Acad. Sci. USA* 104, 10679–10684.
- Muslimov, I.A., Banker, G., Brosius, J., and Tiedge, H. (1998). Activity-dependent regulation of dendritic BC1 RNA in hippocampal neurons in culture. *J. Cell Biol.* 141, 1601–1611.
- Ng, S.Y., Bogu, G.K., Soh, B.S., and Stanton, L.W. (2013). The long noncoding RNA RMST interacts with SOX2 to regulate neurogenesis. *Mol. Cell* 51, 349–359.
- Nie, Y., Tian, G.G., Zhang, L., Lee, T., Zhang, Z., Li, J., and Sun, T. (2021). Identifying cortical specific long noncoding RNAs modified by m(6)A RNA methylation in mouse brains. *Epigenetics* 16, 1260–1276.
- Pan, X., Zhao, J., Zhou, Z., Chen, J., Yang, Z., Wu, Y., Bai, M., Jiao, Y., Yang, Y., Hu, X., et al. (2021). 5'-UTR SNP of FGF13 causes translational defect and intellectual disability. *Elife* 10, e63021.
- Perry, R.B.T., Hezroni, H., Goldrich, M.J., and Ulitsky, I. (2018). Regulation of neuroregeneration by long noncoding RNAs. *Mol. Cell* 72, 553–567.e5. e555.
- Poulopoulos, A., Murphy, A.J., Ozkan, A., Davis, P., Hatch, J., Kirchner, R., and Macklis, J.D. (2019). Subcellular transcriptomes and proteomes of developing axon projections in the cerebral cortex. *Nature* 565, 356–360.
- Quan, Z., Zheng, D., and Qing, H. (2017). Regulatory roles of long non-coding RNAs in the central nervous system and associated neurodegenerative diseases. *Front. Front. Cell. Neurosci.* 11, 175.
- Qureshi, I.A., Mattick, J.S., and Mehler, M.F. (2010). Long non-coding RNAs in nervous system function and disease. *Brain Res.* 1338, 20–35.
- Ramos, A.D., Andersen, R.E., Liu, S.J., Nowakowski, T.J., Hong, S.J., Gertz, C., Salinas, R.D., Zarabi, H., Kriegstein, A.R., and Lim, D.A. (2015). The long noncoding RNA Pnky regulates neuronal differentiation of embryonic and postnatal neural stem cells. *Cell Stem Cell* 16, 439–447.
- Raveendra, B.L., Swarnkar, S., Avchalumov, Y., Liu, X.A., Grinman, E., Badal, K., Reich, A., Pascal, B.D., and Puthanveettil, S.V. (2018). Long noncoding RNA GM12371 acts as a transcriptional regulator of synapse function. *Proc. Natl. Acad. Sci. USA* 115, E10197–E10205.
- Ries, R.J., Zaccara, S., Klein, P., Olarerin-George, A., Namkoong, S., Pickering, B.F., Patil, D.P., Kwak, H., Lee, J.H., and Jaffrey, S.R. (2019). m(6)A enhances the phase separation potential of mRNA. *Nature* 571, 424–428.
- Shi, H., Wang, X., Lu, Z., Zhao, B.S., Ma, H., Hsu, P.J., Liu, C., and He, C. (2017). YTHDF3 facilitates translation and decay of N(6)-methyladenosine-modified RNA. *Cell Res.* 27, 315–328.
- Shi, H., Zhang, X., Weng, Y.L., Lu, Z., Liu, Y., Lu, Z., Li, J., Hao, P., Zhang, Y., Zhang, F., et al. (2018). m(6)A facilitates hippocampus-dependent learning and memory through YTHDF1. *Nature* 563, 249–253.
- Su, Y.Y., Ye, M., Li, L., Liu, C., Pan, J., Liu, W.W., Jiang, Y., Jiang, X.Y., Zhang, X., Shu, Y., and Bao, L. (2013). KIF5B promotes the forward transport and axonal function of the voltage-gated sodium channel Nav1.8. *J. Neurosci.* 33, 17884–17896.
- Takei, Y., Teng, J., Harada, A., and Hirokawa, N. (2000). Defects in axonal elongation and neuronal migration in mice with disrupted tau and map1b genes. *J. Cell Biol.* 150, 989–1000.

- Taverna, E., Götz, M., and Huttner, W.B. (2014). The cell biology of neurogenesis: toward an understanding of the development and evolution of the neocortex. *Annu. Rev. Cell Dev. Biol.* 30, 465–502.
- Tseng, Y.Y., Moriarity, B.S., Gong, W., Akiyama, R., Tiwari, A., Kawakami, H., Ronning, P., Reuland, B., Guenther, K., Beadnell, T.C., et al. (2014). PVT1 dependence in cancer with MYC copy-number increase. *Nature* 512, 82–86.
- Wang, B., Pan, L., Wei, M., Wang, Q., Liu, W.W., Wang, N., Jiang, X.Y., Zhang, X., and Bao, L. (2015a). FMRP-mediated axonal delivery of miR-181d regulates axon elongation by locally targeting Map1b and Calm1. *Cell Rep.* 13, 2794–2807.
- Wang, J.Y., and Lu, A.Q. (2021). The biological function of m6A reader YTHDF2 and its role in human disease. *Cancer Cell Int.* 21, 109.
- Wang, K., Wang, S., Chen, Y., Wu, D., Hu, X., Lu, Y., Wang, L., Bao, L., Li, C., and Zhang, X. (2021a). Single-cell transcriptomic analysis of somatosensory neurons uncovers temporal development of neuropathic pain. *Cell Res.* 31, 904–918.
- Wang, L., Zhao, Y., Bao, X., Zhu, X., Kwok, Y.K.Y., Sun, K., Chen, X., Huang, Y., Jauch, R., Esteban, M.A., et al. (2015b). LncRNA Dum interacts with Dnmts to regulate Dppa2 expression during myogenic differentiation and muscle regeneration. *Cell Res.* 25, 335–350.
- Wang, L.Q., Zheng, Y.Y., Zhou, H.J., Zhang, X.X., Wu, P., and Zhu, S.M. (2021b). LncRNA-Fendrr protects against the ubiquitination and degradation of NLRC4 protein through HERC2 to regulate the pyroptosis of microglia. *Mol. Med.* 27, 39.
- Wang, X., Arai, S., Song, X., Reichart, D., Du, K., Pascual, G., Tempst, P., Rosenfeld, M.G., Glass, C.K., and Kurokawa, R. (2008). Induced ncRNAs allosterically modify RNA-binding proteins in cis to inhibit transcription. *Nature* 454, 126–130.
- Wang, X., Liu, C., Zhang, S., Yan, H., Zhang, L., Jiang, A., Liu, Y., Feng, Y., Li, D., Guo, Y., et al. (2021c). N(6)-methyladenosine modification of MALAT1 promotes metastasis via reshaping nuclear speckles. *Dev. Cell* 56, 702–715.e8. e708.
- Wang, X., Zhao, B.S., Roundtree, I.A., Lu, Z., Han, D., Ma, H., Weng, X., Chen, K., Shi, H., and He, C. (2015c). N(6)-methyladenosine modulates messenger RNA translation efficiency. *Cell* 161, 1388–1399.
- Wei, M., Huang, J., Li, G.W., Jiang, B., Cheng, H., Liu, X., Jiang, X., Zhang, X., Yang, L., Bao, L., and Wang, B. (2021). Axon-enriched lincRNA ALAE is required for axon elongation via regulation of local mRNA translation. *Cell Rep.* 35, 109053.
- Wen, S., Wei, Y., Zen, C., Xiong, W., Niu, Y., and Zhao, Y. (2020). Long non-coding RNA NEAT1 promotes bone metastasis of prostate cancer through N6-methyladenosine. *Mol. Cancer* 19, 171.
- Weng, Y.L., Wang, X., An, R., Cassin, J., Vissers, C., Liu, Y., Liu, Y., Xu, T., Wang, X., Wong, S.Z.H., et al. (2018). Epitranscriptomic m(6)A regulation of axon regeneration in the adult mammalian nervous system. *Neuron* 97, 313–325.e6. e316.
- Widagdo, J., and Anggono, V. (2018). The m6A-epitranscriptomic signature in neurobiology: from neurodevelopment to brain plasticity. *J. Neurochem.* 147, 137–152.
- Wu, P., Zuo, X., Deng, H., Liu, X., Liu, L., and Ji, A. (2013). Roles of long non-coding RNAs in brain development, functional diversification and neurodegenerative diseases. *Brain Res. Bull.* 97, 69–80.
- Xiao, Y., Wang, Y., Tang, Q., Wei, L., Zhang, X., and Jia, G. (2018). An elongation- and ligation-based qPCR amplification method for the radiolabeling-free detection of locus-specific N(6) -methyladenosine modification. *A. Chem. Int. Ed. Engl.* 57, 15995–16000.
- Xie, X., Wang, S., Li, M., Diao, L., Pan, X., Chen, J., Zou, W., Zhang, X., Feng, W., and Bao, L. (2021). alpha-TubK40me3 is required for neuronal polarization and migration by promoting microtubule formation. *Nat. Commun.* 12, 4113.
- Yao, R.W., Wang, Y., and Chen, L.L. (2019). Cellular functions of long noncoding RNAs. *Nat. Cell Biol.* 21, 542–551.
- Yau, K.W., van Beuningen, S.F.B., Cunha-Ferreira, I., Cloin, B.M.C., van Battum, E.Y., Will, L., Schätzle, P., Tas, R.P., van Krugten, J., Katrukha, E.A., et al. (2014). Microtubule minus-end binding protein CAMSAP2 controls axon specification and dendrite development. *Neuron* 82, 1058–1073.
- Yoon, K.J., Ringeling, F.R., Vissers, C., Jacob, F., Pokrass, M., Jimenez-Cyrus, D., Su, Y., Kim, N.S., Zhu, Y., Zheng, L., et al. (2017). Temporal control of mammalian cortical neurogenesis by m(6)A methylation. *Cell* 171, 877–889.e17. e817.
- Yu, J., Chen, M., Huang, H., Zhu, J., Song, H., Zhu, J., Park, J., and Ji, S.J. (2018). Dynamic m6A modification regulates local translation of mRNA in axons. *Nucleic Acids Res.* 46, 1412–1423.
- Zhao, X., Tang, Z., Zhang, H., Atianjoh, F.E., Zhao, J.Y., Liang, L., Wang, W., Guan, X., Kao, S.C., Tiwari, V., et al. (2013). A long noncoding RNA contributes to neuropathic pain by silencing Kcnq2 in primary afferent neurons. *Nat. Nat. Neurosci.* 16, 1024–1031.
- Zhuang, M., Li, X., Zhu, J., Zhang, J., Niu, F., Liang, F., Chen, M., Li, D., Han, P., and Ji, S.J. (2019). The m6A reader YTHDF1 regulates axon guidance through translational control of Robo3.1 expression. *Nucleic. Nucleic Acids Res.* 47, 4765–4777.

STAR★METHODS

KEY RESOURCES TABLE

REAGENT or RESOURCE	SOURCE	IDENTIFIER
Antibodies		
Rabbit polyclonal anti-m ⁶ A	Synaptic Systems	Cat#:202003; Lot.2-96
Rabbit monoclonal anti-YTHDF1	Abcam	Cat#:ab220162; GR3261074-5
Rabbit polyclonal anti-YTHDF3	Abcam	Cat#:ab220161; GR3297561-1
Mouse monoclonal anti-tubulin	Sigma-Aldrich	Cat#:T5168; 038M4813V
Mouse monoclonal anti-Tau	Chemicon	Cat#: MAB3420; RRID: AB_94855
Chicken polyclonal anti-Tuj1	Abcam	Cat#: ab107216; RRID: AB_10899689
Rabbit monoclonal anti-Tau	Abcam	Cat#:ab32057; RRID: Lot. GR3254929-14
Rabbit polyclonal anti-ribosomal protein L4	Proteintech	Cat#:11302-1-AP; RRID:00,011,666
Rabbit polyclonal anti-YTHDF1	Proteintech	Cat#:17479-1-AP; RRID:lot.00092060
Mouse monoclonal anti-calmodulin	Millipore	Cat#: 05-173; RRID: AB_309644
Mouse monoclonal anti-GAPDH	Abcam	Cat#: ab8245; RRID: AB_2107448
Rabbit polyclonal anti-YTHDF3	abclonal	Cat#: a8395; RRID:lot.0202730101
Mouse monoclonal anti-puromycin	Millipore	Cat# MABE343, RRID: AB_2566826
Goat anti-Mouse IgG HRP conjugate	Chemicon	Cat#: 24031340; RRID: N/A
Goat anti-Rabbit IgG HRP conjugate	Chemicon	Cat#: 24070101; RRID: N/A
Goat anti-Rabbit Secondary Antibody, Alexa Fluor 488	Invitrogen	Cat#: A-11034; RRID: AB_2576217
Goat anti-Mouse Secondary Antibody, Alexa Fluor 488	Invitrogen	Cat# A-21042; RRID: AB_2535711
Goat anti-Rabbit Secondary Antibody, Alexa Fluor 555	Invitrogen	Cat# A-21430; RRID: AB_2535851
Goat anti-Chicken Secondary Antibody, Alexa Fluor 647	Invitrogen	Cat# A-21449; RRID: AB_2535866
Chemicals, peptides, and recombinant proteins		
Ribonucleoside Vanadyl Complex	NEB	Cat#: S1420S
cOmplete TM ULTRA Tablets, Mini, EASYpack Protease Inhibitor Cocktail	Roche	Cat#: 5892970001
Lipofectamine TM 2000 Transfection Reagent	Invitrogen	Cat#: 11668019
Lipofectamine TM RNAiMAX Transfection Reagent	Invitrogen	Cat#: 13778150
DAPI	Invitrogen	Cat#: D1306
Triton X-100	Sangon Biotech	Cat#: A110694
NP40	Sangon Biotech	Cat#: A100777
BSA	ABCone	Cat#: B24726
Actinomycin D	MedChemExpress	Cat#: HY-17559
Puromycin	Sigma-Aldrich	Cat#: p8833
Paraformaldehyde	Sinopharm Chemical Reagent Co., Ltd	Cat#: 80096618
Critical commercial assays		
Hieff Clone One Step Cloning Kit	Yeasen	Cat#: 10911ES25
KOD-Plus-Neo kit	Toyobo	Cat#: F1066K
SuperScript III Reverse Transcriptase	Invitrogen	Cat#: 18080044
PrimeScript RT reagent Kit (Perfect Real Time)	Takara	Cat#: RR037A
Hieff [®] qPCR SYBR Green Master Mix (Low Rox Plus)	Yeasen	Cat#: 11202ES03
Alexa Fluor TM 555 Tyramide SuperBoost TM Kit, goat anti-mouse IgG	Invitrogen	Cat#: B40913
Duolink TM In Situ detection Regents Red	Sigma-Aldrich	Cat#: DUO92008
Duolink TM In Situ PLA [®] Probe Anti-Rabbit PLUS	Sigma-Aldrich	Cat#: DUO92002
Duolink TM In Situ PLA [®] Probe Anti-Mouse MINUS	Sigma-Aldrich	Cat#: DUO92004
Duolink TM In Situ Wash Buffers, Fluorescence	Sigma-Aldrich	Cat#: DUO82049

(Continued on next page)

Continued

REAGENT or RESOURCE	SOURCE	IDENTIFIER
Deposited data		
RNA-seq raw files	This paper	GEO: GSE153164 and GSE155622
Experimental models: cell lines		
N2A	Cell bank of Chinese Academy of Sciences	Cat#: TCM29
ND7/23	Cell bank of Chinese Academy of Sciences	Cat#: 3101ETCSCSP5026
Experimental models: organisms/strains		
Mice: C57BL/6	Shang laboratory animal research center, Chinese academy of sciences	N/A
Oligonucleotides		
See Table S2 for DNA and siRNA used in this paper	This paper	N/A
Recombinant DNA		
pEGFP-N3- <i>Dubr</i> iso1	This paper	N/A
pEGFP-N3- <i>Dubr</i> iso2	This paper	N/A
pEGFP-N3- <i>Dubr</i> iso1 m ⁶ A ^{Mut}	This paper	N/A
pEGFP-N3- <i>Dubr</i> iso2 m ⁶ A ^{Mut}	This paper	N/A
pEGFP-N3- <i>Dubr</i> iso1 m ⁶ A ^{MutR}	This paper	N/A
pEGFP-N3- <i>Dubr</i> iso2 m ⁶ A ^{MutR}	This paper	N/A
pcDNA3.1-YTHDF1	This paper	N/A
pcDNA3.1-YTHDF3	This paper	N/A
pEGFP-N3	This paper	N/A
pAKD-CMV-H1-shNC	This paper	N/A
pAKD-CMV-H1-sh <i>Dubr</i>	This paper	N/A
Software and algorithms		
Fiji/ImageJ	Fiji/ImageJ	https://imagej.net/Fiji
Prism	GraphPad Software	https://www.graphpad.com/scientificsoftware/prism/

RESOURCE AVAILABILITY

Lead contact

Further information and requests for resources and reagents should be directed to and will be fulfilled by the lead contact, Bin Wang (wangbin@gdiist.cn).

Materials availability

Requests for materials generated in this study should be directed to the lead contact, Bin Wang (wangbin@gdiist.cn), after completing Material Transfer Agreement.

Data and code availability

- This paper analyzes existing single-cell RNA-seq data at GEO. Their accession numbers are listed in the key resources table.
- This paper does not report original code.
- Any additional information required to reanalyze the data reported in this paper is available from the lead contact upon request.

EXPERIMENTAL MODEL AND SUBJECT DETAILS

Animals

All experiments were approved by the Committee of Use of Laboratory Animals in the Shanghai Institute of Biochemistry and Cell Biology, Chinese Academy of Sciences. The C57BL/6 male and female mice at postnatal day 0 were provided by Shanghai Laboratory Animal Center, Chinese Academy of Sciences.

Cell lines

N2A cells and ND7/23 cells were obtained from the Cell bank of Chinese Academy of Sciences and European Collection of Cell Cultures (United Kingdom), respectively. N2A cells were cultured in Dulbecco's modified Eagle's medium (DMEM) (Invitrogen) supplemented with 5% fetal bovine serum (GIBCO) and 0.5% penicillin/streptomycin. ND7/23 cells were cultured in DMEM supplemented with 5% fetal bovine serum, 0.5% penicillin/streptomycin and 1% GlutaMAX.

Primary culture of DRG explants and neurons

Ex-vivo-culture of DRG explants was performed according to the previous study ([Li et al., 2012](#)). Briefly, DRGs were dissected from mice at P0, supplemented with Matrigel matrix (Corning) and plated on the dish pre-coated with 0.5 µg/mL Poly-D-lysine (Sigma). The DRG explants were cultured in the neurobasal medium containing 2% B27 supplement, 2 mM L-glutamine (Invitrogen) and 50 ng/mL nerve growth factor (Invitrogen), and 10 µM 5-fluoro-2'-deoxyuridine (Sigma) was used to inhibit the proliferation of non-neuronal cells. For microfluidic-cultured P0 DRG neurons, DRGs were digested with a mixture enzyme of 1 mg/mL collagenase I, 0.4 mg/mL trypsin and 0.1 mg/mL DNaseI as previously reported ([Wei et al., 2021](#)). The dissociated DRG neurons were plated into the cell body compartment. The axons crossed the microchannels and reached the axon compartment within 24 h.

METHOD DETAILS

Plasmids

The full length of *Dubr* iso1 and iso2 were amplified from mouse cDNA and cloned into pcDNA3.1, and all m⁶A mutations of *Dubr* were generated using KOD-Plus-Mutagenesis Kit (TOYOBO). The coding sequence of YTHDF1 and YTHDF3 were amplified from mouse cDNA and cloned into pcDNA3.1 to produce pcDNA3.1-YTHDF1 and pcDNA3.1-YTHDF3. shRNA for *Dubr* and the negative control shRNA were cloned into the pAKD-CMV-bGlobin-eGFP-H1-shRNA, respectively.

Cell transfection

Transfection of plasmids was performed with lipofectamine 2000 (Invitrogen) according to the manufacturer's protocol. siRNA transfection was carried out with RNAiMAX (Invitrogen) according to the manufacturer's protocol. For electroporation of P0 DRG neurons, cells were suspended in electroporation buffer and then electroporated by Nucleofector II (Amaxa) using the program named O-003. siRNA was synthesized (Guangzhou RiboBio Co. Ltd., China). The sequences of *Dubr* and YTHDF1/3 siRNA were indicated in [Table S2](#).

For local transfection of *Dubr*^R in the axon compartment of microfluidic cultured P0 DRG neurons, we obtained the *Dubr*^R RNA by *in vitro* transcription as previously reported ([Wei et al., 2021](#)). Briefly, double stand DNA of *Dubr*^R without si*Dubr* targeting region was amplified from pcDNA-*Dubr* attached with T7 sequence in 5' end. After purified by ethanol, *Dubr*^R RNA was transcribed by using T7 polymerase (Promega). For the rescue experiment of *Dubr*^R, 10 pg *Dubr*^R RNA was mixed with the si*Dubr* in Opti-MEM medium. After mixture with RNAiMax (Invitrogen) for 15 min, they were added to the axon compartment of microfluidic cultured P0 DRG neurons.

RNA extraction, RT-PCR and qPCR

Total RNA was extracted from tissues or cultured cells with TRIzol reagent according to the manufacturer's protocol (Invitrogen). To obtain the RNA from the cell body and axon, the TRIzol reagent was used to dissolve tissues in the cell body and axon compartment, respectively. Three microfluidic chambers were collected for the axonal RNA dissolved in 5 µL RNase free water whereas the RNA from cell bodies dissolved in 50 µL RNase free water. The RNA was then treated with gDNA eraser to degrade possible genomic DNA pollution before reverse-transcription with the PrimerScript RT Reagent Kit (TaKaRa). For the reverse transcription, total axonal RNA and 1% cell body RNA were used in cDNA synthesis for qPCR analysis. Then, the cDNA synthesis was carried out with oligo (dT) and random hexamers. qPCR was performed using HieffTM qPCR SYBR Green Master Mix (Yeasen) and Lightcycler R 96 System (Roche). The data were analyzed and normalized to *Gapdh* mRNA for the relative level of mRNA or lincRNA, which were then converted into the fold change. For heatmap, the relative expression level for individual lincRNA at different stages were calculated by normalizing to its highest expression stage. Primer sequences for qPCR were provided in [Table S2](#).

Immunostaining

DRG neurons plated on the dish or the microfluidic devices were fixed in 4% paraformaldehyde for 15 min at room temperature. Then, the neurons were incubated with the indicated primary antibodies overnight at 4°C followed by secondary antibodies conjugated with fluorescent dye (1:1000; Jackson Immunoresearch) and DAPI (1:2000; Sigma) for 45 min at 37°C.

The immunostaining for the brain sections was performed as previously reported ([Xie et al., 2021](#)). Briefly, the brain tissues of E18 and P3 mice were dissected, post-fixed with 4% paraformaldehyde for 24 h, and dehydrated in 30% sucrose overnight at 4°C. The 50 µm-thick sections were cut by a cryostat and incubated with indicated primary antibodies diluted in the buffer containing 1% BSA and 0.3% Triton X-100 against for 24 h at 4°C. The sections were then incubated with Alexa-Fluor-conjugated secondary antibodies (1:1000; Jackson Immunoresearch) and DAPI (1:2000; Sigma) for 2 h at room temperature and mounted on gelatin-coated slides. All images of immunostaining were acquired from Nikon A1R confocal microscope (Nikon).

Immunoblotting

Tissues, cell lysates or beads were incubated in SDS-PAGE loading buffer for 5 min at 95°C. The samples were separated on SDS-PAGE, transferred to the nitrocellulose membrane (Whatman), blocked by 5% milk for 40 min at room temperature probed with specific antibodies, and visualized with enhanced chemiluminescence (Amersham Biosciences). The intensity of immunoreactive bands was analyzed with the Image-Pro Plus 5.1 software (Media Cybernetics).

In situ hybridization

The subcellular detection of *Dubr* was performed as previously described (Wang et al., 2015a). Briefly, antisense probe for *Dubr* amplified with PCR primers and labeled with DIG. The cultured P0 DRG neurons were fixed in 4% paraformaldehyde and hybridized at 65°C overnight. After incubation with anti-DIG-POD (Roche) at 4°C overnight, the signal was amplified by TSA™ Plus Cy3 System (PerkinElmer Inc.). For immunostaining, the neurons were incubated with the indicated primary antibody overnight at 4°C followed by secondary antibodies conjugated with fluorescent dye for 45 min at 37°C before TSA amplification. The cells were scanned by Nikon A1R confocal microscope (Nikon).

Axon elongation assay

The elongated axon growth was measured as described previously (Wei et al., 2021). Briefly, in ex-vivo-culture of P0 DRG explants, the images for axons extending from DRG explants were captured after siRNA treatment for 48 h by Zeiss LSM 880 (Zeiss) and the elongated length was analyzed by ImageJ (NIH). In microfluidic-cultured P0 DRG neurons, the neurons electroporated with GFP to clearly visualize the process of axon elongation were transfected with siRNA and plasmids in the cell body compartment or axon compartment. The images of axons in the axon compartment were captured by Zeiss LSM 880 (Zeiss). Then, each photograph was stitched to produce an integrated image for whole axon compartment. After 24 h, the second image was produced at the same axon compartment. The increase of single axon length clearly detected during 24 h was analyzed using the plug-in of Simple neurite tracer from ImageJ (NIH). At least 3 chambers and total 150 axons per group in 3 independent experiments were performed for quantitative analysis. For analysis of axon projection from cortical neurons, the distance was measured according to axon positions at the midline by ImageJ (NIH). Quantitative data were collected from at least 3 brains under each experimental condition.

In utero electroporation

In utero electroporation of embryonic E14 mice was performed as previously reported (Xie et al., 2021). Briefly, 0.75 µg GFP and 0.1 µL of Fast Green (2 mg/mL; Sigma) mixed with 3 µg of indicated plasmids were injected into lateral ventricle of the embryo. The electric pulses were generated by an ElectroSquireportator T830 (BTX) and applied to the cerebral wall for 5 repetitions of 30 V for 50 ms with an interval of 1 s. After the electronation, the uterus was returned to the abdominal cavity. At E18 or P3, the mouse brains were dissected and performed by immunostaining.

Three to ten puppy brains were from at least 3 individual mothers in each group were used to the quantitative analysis of neuronal position. The fluorescence images captured from the somatosensory cortex were used to analyze the radial migration of cortical neurons. The different subregions of cortical wall were identified based on cell density after staining with DAPI. At least 3 brains under each experimental condition were used to quantitative analysis.

Immunoprecipitation and RNA immunoprecipitation (RIP)

ND7/23 cells or DRG tissues were harvested and lysed with RIPA buffer (20 mM Tris-HCl, 150 mM NaCl, 1 mM NaF, 1 mM MgCl₂, 1 mM DTT, 0.5% NP-40) with RNase inhibitor (Promega) and protease inhibitor cocktail (Roche). The resulting supernatant was incubated with 1 µg antibody at 4°C for 2 h in the RIPA buffer. Then, the 50 µL protein G beads (Sigma) were incubated with lysates and antibody at 4°C for 1 h in the RIPA buffer. The same amount of IgG was used as a control. The protein-captured beads were washed with the RIPA buffer for 3 times. RNA extraction and immunoblotting from the beads were further performed by using TRIzol (Invitrogen) and loading buffer, respectively, for subsequent detection of co-immunoprecipitated RNA and protein. For the normalization of immunoprecipitates (Figures 7A–7C), more volume of immunoprecipitated samples were loaded to guarantee the equal amounts of YTHDF1 as a loading control. The original intensities of immunoblots for YTHDF3 and IgG were normalized by YTHDF1.

The SELECT detection assay

SELECT assay was performed by Epi-SELECT m⁶A site identification kit with FTO assist step (Guangzhou Epibiotek Co., Ltd.) as previously described (Xiao et al., 2018). Briefly, 1 µg total RNA of ND7/23 cell was mixed with 5 µL FTO, 10 µL 5× FTO reaction buffer, 1 µL RI, RNase-free Water to 50 µL. Then the RNA and FTO were annealed by incubating the mixture at a temperature gradient: 37°C for 30min, 4°C hold, 4 µL 0.5 M EDTA denatured at 95°C for 5 min. Afterward, RNA was mixed with 1 µM Up Primer, 1 µM Down Primer and 5 µM dNTP in 17 µL 1× CutSmart buffer. Subsequently, 3 µL of mixture containing 0.3 µL SELECT™ DNA polymerase, 0.47 µL SELECT™ ligase and 2.23 µL ATP was added to the former mixture to 20 µL. The final reaction mixture was incubated at 40°C for 20 min and denatured at 80°C for 20 min qPCR was performed using HieffTM qPCR SYBR Green Master Mix (Yeasen) and Light-cycler R 96 System (Roche). Primer sequences for specific m⁶A sites of *Dubr* are listed in Table S2.

Detection of protein stability

The CHX chase assay was performed to detect the protein stability as previously reported with minor modifications (Su et al., 2013). Briefly, 60 µg/mL CHX (Sigma) was added for 1, 2, 3 and 4.5 h in ND7/23 cells after transfected with siRNA for 48 h, respectively. 10 µM MG132 (Sigma) and 25 mM NH4Cl (Sigma) were used to inhibit proteasome- and lysosome-dependent protein degradation pathway, respectively. Immunoblotting was further carried out to examine the protein level. In all experiments, the control group was treated with the vehicle used for drug preparation.

Puromycylation-PLA assay

The puromycylation-PLA assay was performed to detect the nascent protein according to previous study (Wei et al., 2021). Briefly, cultured P0 DRG neurons after transfected with siRNA for 48 h were treated with CHX (100 µg/mL) for 30 min at 37°C. Then, the cells were incubated with the medium containing 1 µM puromycin (Sigma) for 10 min at 37°C and fixed with 4% paraformaldehyde for 20 min. The following PLA detection was carried out by Duolink reagents (Sigma) according to the manufacturer's instructions. Detection of newly synthesized Tau by PLA was performed by using anti-Tau and anti-puromycin. The antibody combination was applied to the cells and incubated at 4°C overnight. Then, the cells were incubated with probes including PLA^{minus} and PLA^{plus} in a 1:5 dilution in blocking buffer for 1 h at 37°C, and ligated with T4 ligase for 30 min at 37°C. After ligation, amplification reaction (Sigma) containing polymerase and fluorophore-labeled detection oligo was performed in the cell to initiate and amplify signals for 100 min at 37°C. Finally, cells were incubated with DAPI and then mounted with a coverslip. Images were acquired with Leica SP8 confocal microscope using a 63×/1.4-NA oil objective.

QUANTIFICATION AND STATISTICAL ANALYSIS

Analysis of m⁶A-modified RNAs in the DRG of adult mice

Raw m⁶A-SMART-seq datasets, including two replicates of naive group, were obtained from Weng et al. (Weng et al., 2018). For raw data processing, we first performed adapter trimming and low-quality reads removal with cutadapt (v2.1, parameter: -a CTGTCTCTTATA -a TTTTTT -q 20,20 -m 20) (<https://doi.org/10.14806/ej.17.1.200>). These remaining reads were aligned to mouse genome reference (mm10) by STAR aligner (v2.7.0f, default parameter) (<https://doi.org/10.1093/bioinformatics/bts635>). Then, read counts of genes from GENCODE annotation (M25) was calculated by featureCounts (v1.6.2, parameter: -M -O –fraction) (<https://doi.org/10.1093/bioinformatics/btt656>) and further normalized by transcript per million (TPM). Finally, the ratio of TPM values (m⁶A enriched folds) between m⁶A IP and input conditions per gene was used to reflect the relative m⁶A level on a transcriptome-wide scale. All genes were classified with the tag of “gene_type” in GENCODE reference.

Statistical analysis

All data are presented as the mean ± SEM. Statistical analyses were performed using unpaired *t* test to evaluate effects in single-factor experiments, and two-way ANOVA to determine the effects of each variable in two-factor experiments (GraphPad Software). Differences were considered significant at *p* < 0.05.

Supplemental information

**m⁶A-modified lincRNA *Dubr* is required
for neuronal development by stabilizing
YTHDF1/3 and facilitating mRNA translation**

Jiansong Huang, Bowen Jiang, Guo-Wei Li, Dandan Zheng, Mingyi Li, Xuan Xie, Yuxiang Pan, Manyi Wei, Xiaoyan Liu, Xingyu Jiang, Xu Zhang, Li Yang, Lan Bao, and Bin Wang

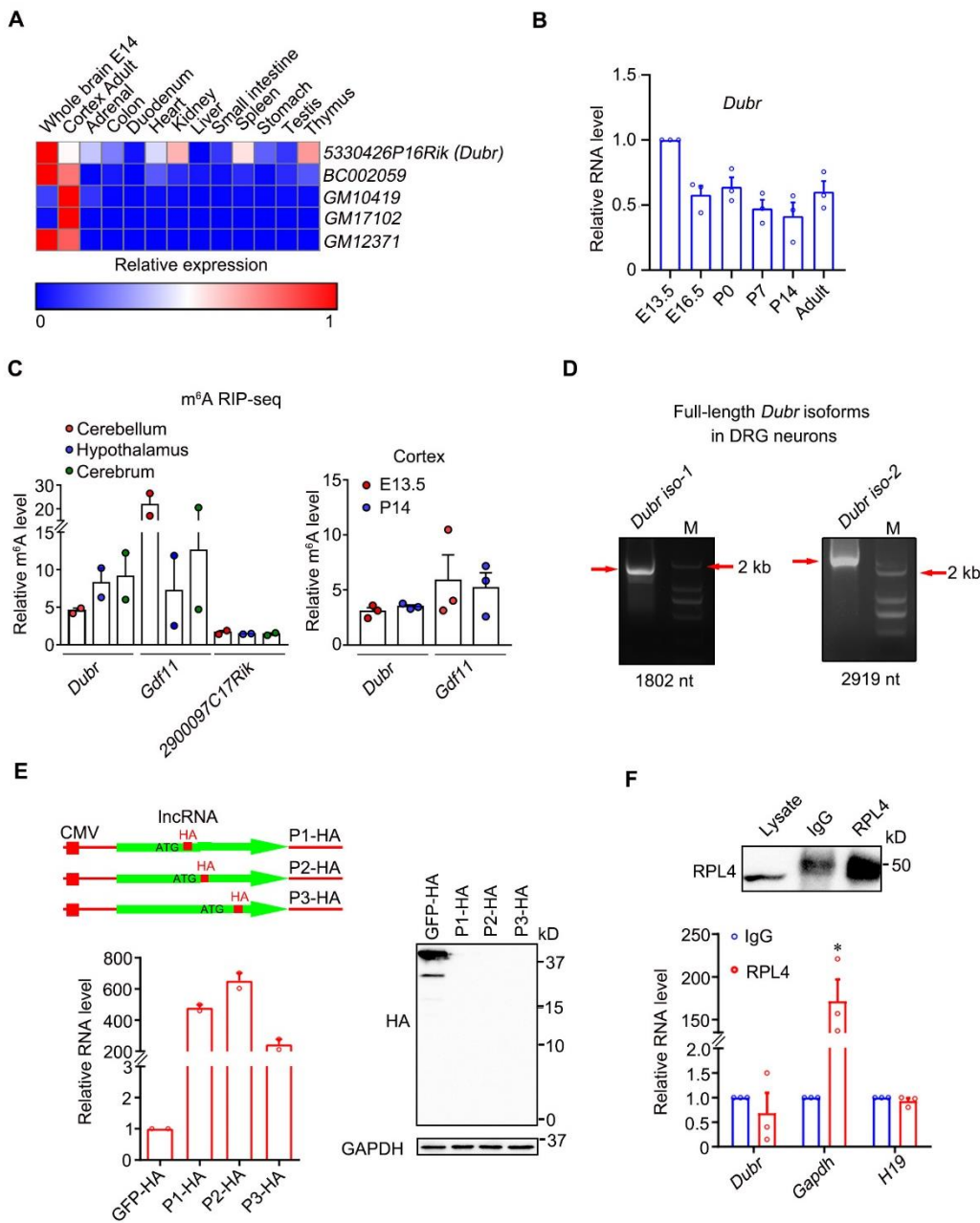


Figure S1. Related to Figure 1, lincRNA *Dubr* is highly enriched in the nervous system.

(A) Heatmap for the RNA-seq of mouse tissues showed that 5 lncRNAs were highly enriched in the nervous system. RNA-seq datasets from mouse tissues were taken from Ensemble database.

(B) PCR analysis showed that expression of *Dubr* decreased progressively in DRGs

from E13.5 to P14. n = 3.

(C) m⁶A-RIP-seq analysis showed that methylation of *Dubr* was enriched in different regions of 7-week mouse brain including cerebellum, hypothalamus and cerebrums (left) as well as the cortex of E13.5 and P14 mice (right). *Gdf1* and *2900097C17Rik* served as a positive and negative control, respectively.

(D) PCR showing the full length of *Dubr iso1* and *iso2* in P0 DRG neurons. The *iso1* and *iso2* of *Dubr* contained 1802 nt and 2919 nt, respectively.

(E) A schematic (up) showing 3 distinct constructs by inserting HA tag after start codon of ORF. qPCR (down left) detected that the exogenous-expressed level of *Dubr* segments were comparable after overexpression of P1-HA, P2-HA, and P3-HA constructs in N2A cells. Representative immunoblots (right) showed that 3 *Dubr* segments did not encode a small peptide. GAPDH served as a loading control.

(F) RIP (up) and qPCR (down) showed that *Dubr* was not enriched in the RPL4 immunoprecipitates of ND7/23 cells. IgG served as a control. *Gapdh* and *H19* served as a positive and negative control, respectively. * P < 0.05 versus IgG. n = 3

All results were shown as the mean ± SEM.

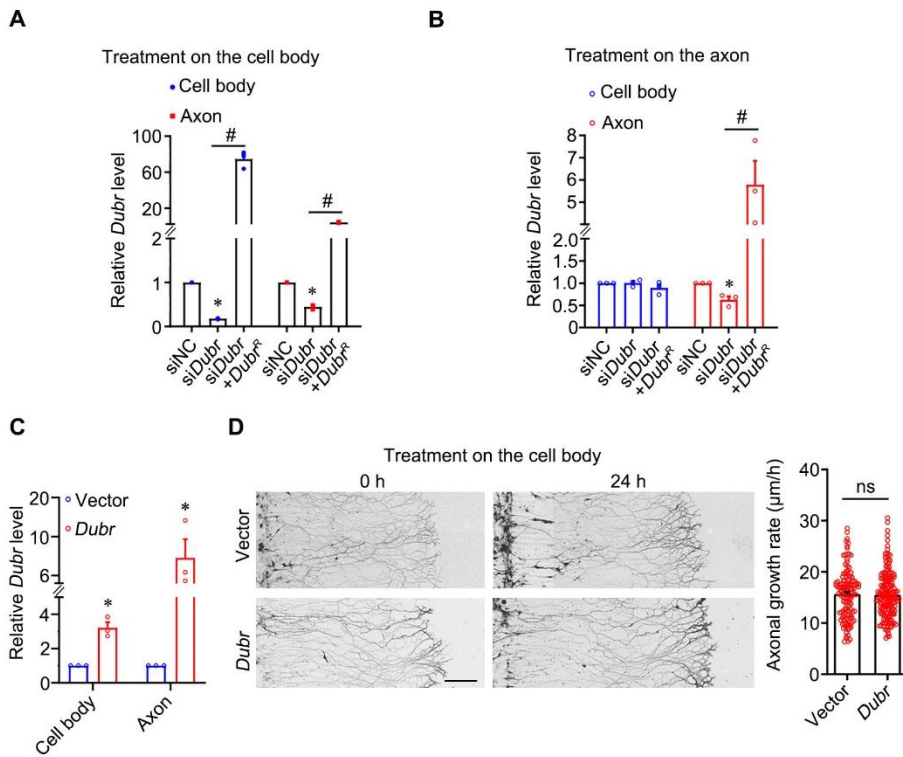


Figure S2. Related to Figure 2, overexpression of *Dubr* does not affect the axon elongation of DRG neurons.

(A) qPCR showed that *siDubr* in the cell body compartment reduced the level of *Dubr* both in cell bodies and axons, while coexpression of *Dubr*^R fully rescued the decreased level of *Dubr* due to *siDubr* treatment. * P < 0.05 versus siNC and # P < 0.05 versus indicated. n = 3.

(B) qPCR showed that *siDubr* in the axon compartment reduced the level of *Dubr* in axons but not in cell bodies, while coexpression of *Dubr*^R in axons fully rescued the decreased level of axonal *Dubr* due to *siDubr* treatment. * P < 0.05 versus siNC and # P < 0.05 versus indicated. n = 3.

(C) qPCR showed that the level of *Dubr* in cell bodies and axons was increased after overexpression of *Dubr* in the cell body compartment of microfluidic-cultured DRG

neurons. * P < 0.05 versus vector. n = 3.

(D) Representative images (left) and quantitative data (right) showed that overexpression of *Dubr* in the cell body compartment did not affect axon elongation (Vector, n = 157; si*Dubr*, n = 187). ns versus indicated. Scale bar, 300 μ m.

All results were shown as the mean \pm SEM.

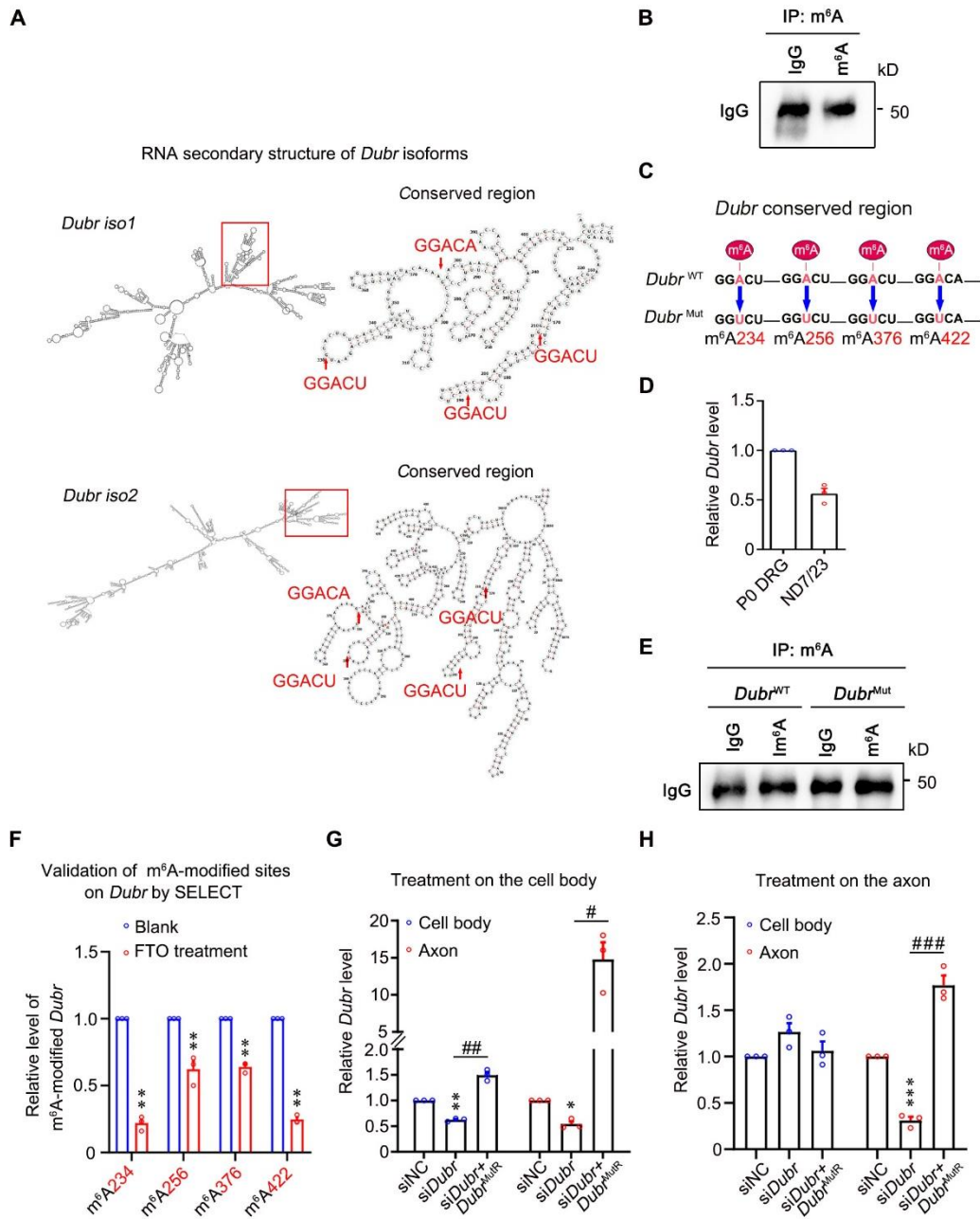


Figure S3. Related to Figure 4, the m⁶A modification motifs of *Dubr*.

(A) Analysis of RNA secondary structure by RNA structure software predicted 4 high-confidence m⁶A-modified motifs within the conserved region of *Dubr* isoforms.

(B) Representative immunoblots showing the similar amount of m⁶A immunoprecipitates in ND7/23 cells. IgG served as a control.

(C) A schematic showing the constructs of *Dubr*^{WT} and *Dubr*^{Mut}. The core alanine (A)

within 4 m⁶A-modified motifs including three GGACU (m⁶A234, m⁶A256 and m⁶A376) and one GGACA (m⁶A422) was mutated to phenylalanine (U) in the construct of *Dubr*^{Mut}.

(D) qPCR showed that the expression of *Dubr* in ND7/23 cells displayed similar level to cultured P0 DRG neurons. n=3.

(E) Representative immunoblots showing the similar amount of m⁶A immunoprecipitates in ND7/23 cells expressing *Dubr*^{WT} or *Dubr*^{Mut}. IgG served as a control.

(F) qPCR showed that FTO significantly decreased the level of m⁶A modification on 4 sites (m⁶A234, m⁶A256, m⁶A376 and m⁶A422) in *Dubr* from the RNA lysates of ND7/23 cells. ** P < 0.01 versus Blank. n = 3.

(G) qPCR showed that transfection of si*Dubr* in the cell body compartment decreased expression level of *Dubr* in cell bodies and axons, and coexpression of *Dubr*^{MutR} in cell bodies completely rescued the decreased *Dubr* level due to si*Dubr*. * P < 0.05, ** P < 0.01 versus siNC and # P < 0.05, ## P < 0.01 versus indicated. n = 3.

(H) qPCR showed that transfection of si*Dubr* in the axon compartment decreased expression level of *Dubr* in axons, and coexpression of *Dubr*^{MutR} in axons completely rescued the decreased *Dubr* level due to si*Dubr*, whereas the level of *Dubr* in cell bodies remained unchanged. *** P < 0.001 versus siNC and ### P < 0.001 versus indicated. n = 3.

All results were shown as the mean ± SEM.

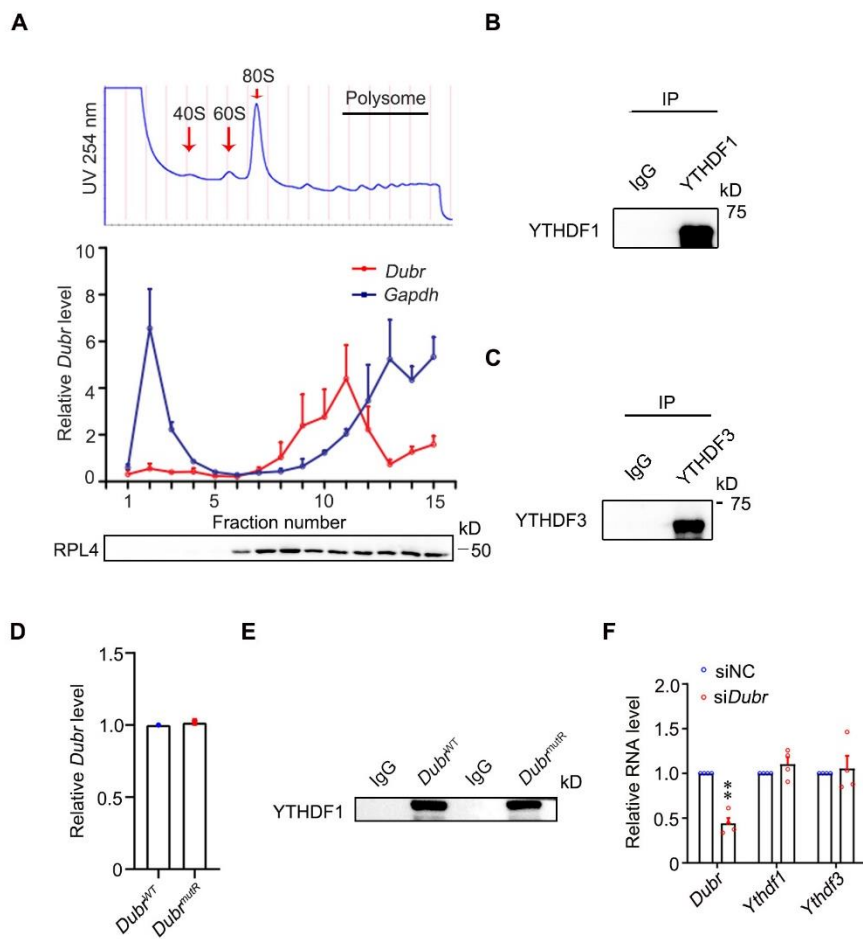


Figure S4. Related to Figure 5, *Dubr* is polysome-enriched and associates with YTHDF1/3.

(A) qPCR showed that *Dubr* was mainly distributed in the 80s and polyribosome fractions. *Gapdh* and *RPL4* served as a polysome-enriched RNA and ribosome protein, respectively. n = 3.

(B and C) Representative immunoblots showed that YTHDF1 and YTHDF3 were greatly enriched in the YTHDF1 (B) and YTHDF3 (C) immunoprecipitates of ND7/23 cells.

(D) qPCR showing the similar level of *Dubr* in ND7/23 cells expressing *Dubr*^{WT} or

Dubr^{MutR}. n = 3.

(E) Representative immunoblots showing the similar amount of YTHDF1 immunoprecipitates in ND7/23 cells expressing *Dubr*^{WT} or *Dubr*^{MutR}.

(F) qPCR showed that the mRNA levels of *Ythdf1* and *Ythdf3* were not affected by si*Dubr*. ** P < 0.01 versus siNC. n = 4.

All results are presented as the mean ± SEM.

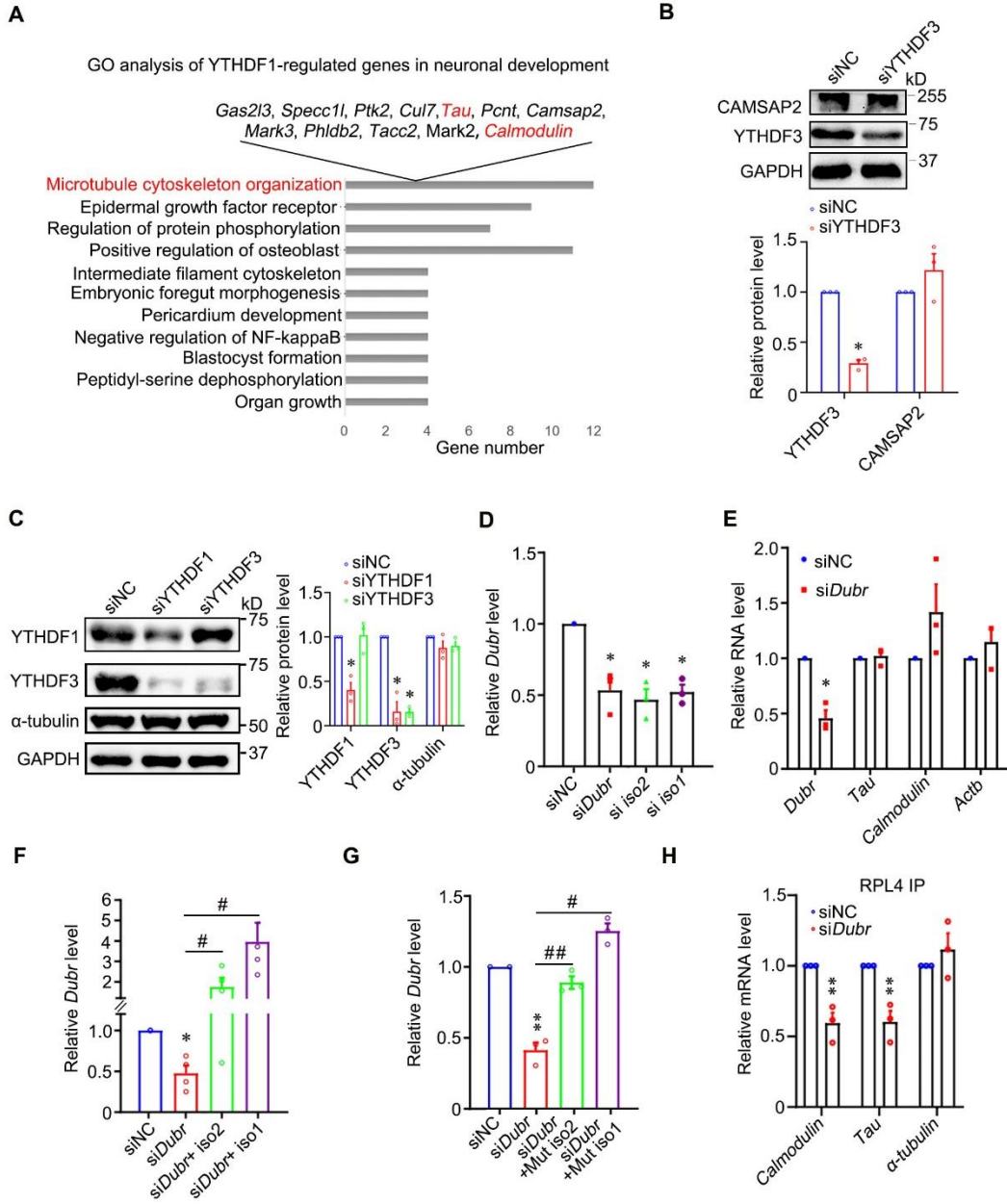


Figure S5. Related to Figure 6, Dubr downregulation affects mRNA translation of

***Tau* and *Calmodulin*.**

- (A) GO analysis showed that the potential functions of YTHDF1-associated genes were highly enriched in microtubule cytoskeleton organization.
- (B) Representative immunoblots (up) and quantitative data (down) showed that knockdown of YTHDF3 didn't affect the protein level of CAMSAP2. GAPDH and α -

tubulin served as a loading control and negative control, respectively. * P < 0.05 versus siNC. n = 3.

(C) Representative immunoblots (left) and quantitative data (right) showed that knockdown of YTHDF1 or YTHDF3 decreased the proteins level of Tau and Calmodulin. GAPDH served as a loading control. * P < 0.05 versus siNC. n = 3.

(D) qPCR showed that the expression of *Dubr* was significantly decreased by knocking down either total and each isoform of *Dubr*. n = 3. * P < 0.05 versus siNC.

(E) qPCR showed that mRNAs level of *Tau* and *Calmodulin* were not affected by si*Dubr*. * P < 0.05 versus siNC. n = 4.

(F and G) qPCR showed that the decreased *Dubr* was fully rescued by coexpression of *Dubr* isoform 1 or 2 (F) and *Dubr*^{Mut} isoform 1 or 2 (G) in cultured P0 DRG neurons, respectively. * P < 0.05, ** P < 0.01 versus siNC and # P < 0.05, ## P < 0.01 versus indicated. n = 4.

(H) qPCR (right) showed that mRNAs level of *Tau* and *Calmodulin* were decreased in the RPL4 immunoprecipitates of ND7/23 cells. IgG served as a control. *a-tubulin* served as a negative control. ** P < 0.01 versus siNC. n = 3.

All results were shown as the mean ± SEM.

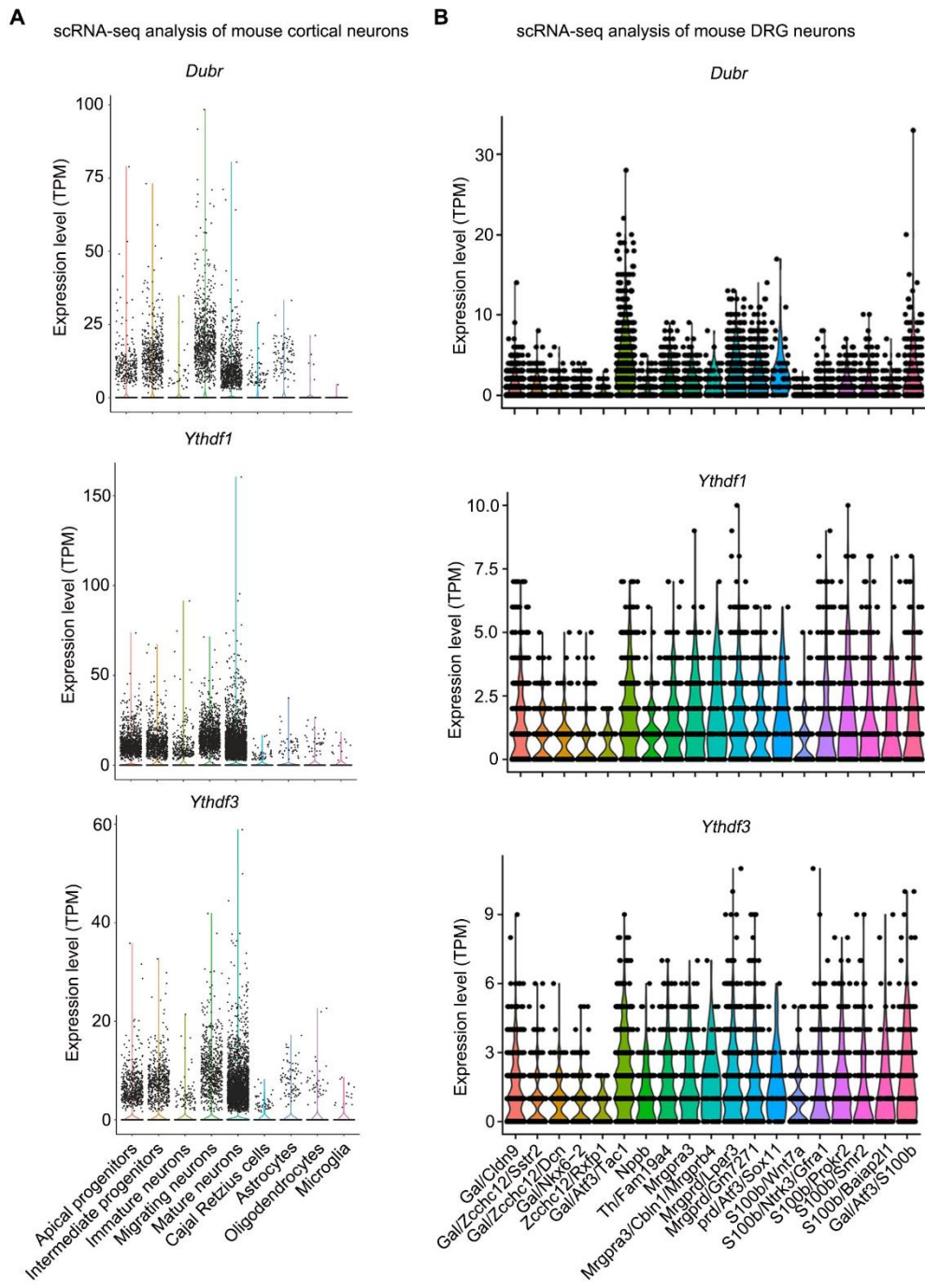


Figure S6. Related to Figure 7, scRNA-seq shows that *Ythdf1*, *Ythdf3* and *Dubr* are coexpressed in cortical and DRG neurons.

(A) scRNA-seq analysis showed that *Dubr*, *Ythdf1* and *Ythdf3* were coexpressed in the types of progenitors (apical and intermediate) and neurons (migrating and mature) from embryonic mouse brain cortex. TPM, transcript per million.

(B) scRNA-seq analysis showed that *Dubr*, *Ythdf1* and *Ythdf3* were coexpressed in all types of adult DRG neurons. TPM, transcript per million.

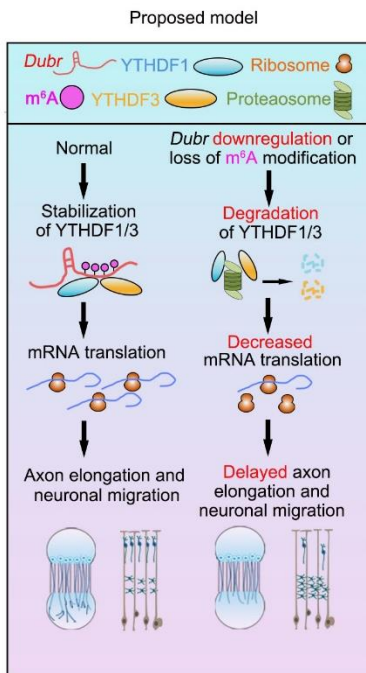


Figure S7. Related to Figure 7, a proposed model for *Dubr* regulating axon elongation and neuronal migration by facilitating YTHDF1/3 stabilization and downstream mRNA translation.

Normally, *Dubr* interacts and stabilizes YTHDF1/3 through its m⁶A modification, thereby facilitating the translation of Tau and Calmodulin as well as maintaining subsequent axon elongation and neuronal migration. When *Dubr* is downregulated during development, YTHDF1/3 are degraded via the proteasome pathway, and the synthesis of Tau and Calmodulin is repressed, then inhibiting axon elongation and neuronal migration.